Technical Document 1632
August 1989

Nuclear Magnetic Resonance Signatures of Nitrogen-Containing Compounds

L. J. Burnett
J. P. Sanders
M. A. Fineman
San Diego State University Foundation

NAVAL OCEAN SYSTEMS CENTER

San Diego, California 92152-5000

E. G. SCHWEIZER, CAPT, USN
Commander

R. M. HILLYER
Technical Director

ADMINISTRATIVE INFORMATION

This work was performed for the Marine Sciences and Technology Department of Naval Ocean Systems Center (NOSC), under program element 62762N. Contract N66001-87-0136 was carried out by the SDSU Foundation, 5178 College Avenue, San Diego, CA 92182-1900, under the technical coordination of A. Nedoluha, NOSC Code 56.

Released under authority of
H. E. Rast, Head
Optical Electronics Branch
and Electronic Material
Sciences Division

MA

REPORT DOCUMENTATION PAGE

1a. REPORT SECURITY CLASSIFICATION UNCLASSIFIED	1b. RESTRICTIVE MARKINGS
2a. SECURITY CLASSIFICATION AUTHORITY	3. DISTRIBUTION/AVAILABILITY OF REPORT Approved for public release; distribution is unlimited.
2b. DECLASSIFICATION/DOWNGRADING SCHEDULE	
4. PERFORMING ORGANIZATION REPORT NUMBER(S)	5. MONITORING ORGANIZATION REPORT NUMBER(S) NOSC TD 1632
6a. NAME OF PERFORMING ORGANIZATION San Diego State University Foundation 6b. OFFICE SYMBOL (if applicable)	7a. NAME OF MONITORING ORGANIZATION Naval Ocean Systems Center Electronic Material Sciences Division
6c. ADDRESS (City, State and ZIP Code) 5178 College Avenue San Diego, California 92182-1900	7b. ADDRESS (City, State and ZIP Code) San Diego, California 92152-5000
8a. NAME OF FUNDING/SPONSORING ORGANIZATION Marine Sciences and Technology Department 8b. OFFICE SYMBOL (if applicable) NOSC Code 50	9. PROCUREMENT INSTRUMENT IDENTIFICATION NUMBER N66001-87-D-0136
8c. ADDRESS (City, State and ZIP Code) Naval Ocean Systems Center San Diego, California 92152-5000	10. SOURCE OF FUNDING NUMBERS PROGRAM ELEMENT NO. 62762N; PROJECT NO. S62588; TASK NO. 560-EE90; AGENCY ACCESSION NO. DN307 379

11. TITLE (include Security Classification)

NUCLEAR MAGNETIC RESONANCE SIGNATURES OF NITROGEN-CONTAINING COMPOUNDS

12. PERSONAL AUTHOR(S)

L. J. Burnett, J. P. Sanders, and M. A Fineman (SDSUF)

13a. TYPE OF REPORT	13b. TIME COVERED	14. DATE OF REPORT (Year, Month, Day)	15. PAGE COUNT
Final	FROM Oct 1987 TO May 1988	August 1989	96

16. SUPPLEMENTARY NOTATION

17. COSATI CODES			18. SUBJECT TERMS (Continue on reverse if necessary and identify by block number)
FIELD	GROUP	SUB-GROUP	nuclear magnetic resonance (NMR); free induction decay (FID); hexamethylenetetramine (HMT); mannitol; Larmor frequency; trinitrotoluene (TNT); pentaerythritol tetranitrate (PETN)

19. ABSTRACT (Continue on reverse if necessary and identify by block number)

Experiments were conducted to determine if unique NMR signatures can be detected and defined for the proton NMR signals of nitrogen-containing compounds. Compounds of particular interest include explosives and explosive stimulants. The effects of off-resonance radio frequency(rf) irradiation, or pumping, were observed in three nitrogen-containing compounds: HMT, TNT, and PETN. Similar effects were observed in mannitol and in the "plastic" explosive C-4, but dielectric heating of the sample C-4 made it impossible to apply the required sequence of rf pulses. The NMR FID signal from C-4 contains two distinct components.

At present, methods to enhance the effects of off-resonance irradiation and improve the NMR signature are not obvious. With proper design, it may be possible to take advantage of the observed effects in field-usable NMR explosive detectors.

20. DISTRIBUTION/AVAILABILITY OF ABSTRACT	21. ABSTRACT SECURITY CLASSIFICATION
☐ UNCLASSIFIED/UNLIMITED ☒ SAME AS RPT ☐ DTIC USERS	UNCLASSIFIED

22a. NAME OF RESPONSIBLE PERSON	22b. TELEPHONE (include Area Code)	22c. OFFICE SYMBOL
D. M. Griffin, COTR	619-553-5460	Code 56

Table of Contents

1 Introduction

The principal objective of this program is to determine if unique nuclear magnetic resonance (NMR) responses, i.e., signatures, can be detected and defined for the proton NMR signals of nitrogen-containing compounds. Compounds of special interest include explosives and explosive simulants.

During the experiments, changes in the proton NMR signals from the samples were observed following irradiation with off-resonance radio frequency (rf) fields. Proton resonance effects were investigated because of the potential for application to present-day NMR explosives detection technology.

The program consisted of four major tasks. Each of these major tasks is summarized below.

Task 1. Construct System. Construct an NMR system and probe suitable for observing proton NMR signals while irradiating the sample at frequencies other than the proton frequency.

Task 2. Investigate Explosive Simulants. Investigate hydrogen-nitrogen NMR off-resonance irradiation effects in one or more explosive simulant compounds, including hexamethylenetetramine.

Task 3. Investigate Explosive Compounds. Investigate hydrogen-nitrogen NMR off-resonance irradiation effects in three or more explosive compounds, including C-4, TNT and PETN.

Task 4. Define Signatures. If possible, define unique NMR signatures for the explosive compounds studied. If appropriate, propose a conceptual design for an NMR detection device that utilizes these signatures.

Each of these tasks was carried out successfully.

This program formed the basis of the thesis work of Mr. John Sanders, who was awarded a Master of Science degree in physics from San Diego State University in May 1988. Mr. Sanders' M.S. thesis is included as Appendix A and details most of the work carried out on this program. To avoid needless duplication, we refer to the discussion, documentation and results contained in this thesis whenever possible.

2 Conclusions

Seven principal conclusions resulted from the studies completed during this program. These seven conclusions are summarized below.

* The effects of off-resonance rf irradiation, or pumping, were observed in three nitrogen-containing compounds: HMT (an explosive simulant), TNT and PETN.

* Similar effects were not observed in mannitol, a compound with similar proton relaxation characteristics which does not contain nitrogen.

* The observed effects in the three nitrogen-containing compounds studied were small but could, in principle, be used to define unique NMR signatures and, in practice, be used to improve the distinction between explosive and benign compounds.

* Similar effects were expected to be observed in the "plastic" explosive C-4, but dielectric heating of the sample made it impossible to apply the required sequence of rf pulses.

* The NMR free induction decay signal from C-4 contains two distinct components.

* At present, methods to enhance the effects of off-resonance irradiation and improve the NMR signature are not obvious.

* With proper design, it may be possible to take advantage of the observed effects in field-usable NMR explosives detectors.

3 Theoretical Principles

In a steady magnetic field, nuclei are found in certain, well-defined energy states or levels. Transitions between levels are governed by rules, called selection rules, which describe the ease of stimulating a particular transition.

For isolated nuclei, transitions are either allowed or forbidden. When allowed transitions are stimulated under certain well-defined conditions, nuclear magnetic resonance (NMR) is the result. When forbidden transitions are stimulated, no NMR response is observed.

When nuclei interact, i.e., when they are not isolated from one another, and when there are several types of nuclei in a particular compound, then transitions that were previously strictly forbidden become weakly allowed. The energies of these weakly-allowed transitions correspond to sums, differences, and multiples of the allowed energies of isolated nuclei. When weakly-allowed transitions are stimulated, it is possible, under certain conditions, to observe weak (often very weak) effects on the NMR response.

Explosive compounds and explosive simulants are prime candidates in searches for the effects of weakly-allowed NMR transitions since these compounds generally contain both hydrogen and nitrogen nuclei in close proximity. The theoretical framework for a description of the effects due to rf pumping of weakly-allowed transitions in hexamethylenetetramine, an explosive simulant, is presented in Appendix A.

The theoretical framework for the effects of off-resonance rf pumping in the explosive compounds studied is also included in Appendix A, with the added complication that, in most explosive compounds, the nitrogen interactions include asymmetry parameters. However, the inclusion of asymmetry parameters does not alter the basic description of the problem.

NMR data were taken on five separate compounds in this study. Each compound possesses distinct NMR characteristics and these are briefly summarized below.

3.1 HMT

Hexamethylenetetramine, or HMT, is sometimes used as an NMR explosive simulant. HMT has a single nitrogen-14 quadrupole coupling constant and an asymmetry parameter of zero [1]. Therefore, HMT has a single NQR frequency, which has a value of 3.308 MHz. Level crossing [2] between hydrogen and nitrogen nuclei occurs in a region of applied field near 780 Gauss.

3.2 Mannitol

Mannitol is a sugar with relaxation characteristics similar to many explosives. That is, it exhibits a long T_1 and a short T_2 [3]. However, mannitol contains no nitrogen nuclei and, therefore, has no nitrogen NQR frequency.

3.3 PETN

PETN has a single quadrupole coupling constant of 0.936 MHz and an asymmetry parameter of 0.855 [1]. This value for the asymmetry parameter was not derived from NQR data, but rather was deduced from structure and crystalline data. PETN should exhibit two NQR frequencies, at 903 KHz and 503 KHz. However, only the 903 KHz line has been observed.

3.4 TNT

Nitrogen nuclei in TNT are found in three distinct sites and, therefore, TNT has three quadrupole coupling constants and asymmetry parameters: 1.081 MHz with an asymmetry parameter of 0.155, 1.107 MHz with an asymmetry parameter of 0.139, and 1.131 MHz with an asymmetry parameter of 0.164 [1].

TNT exhibits six distinct NQR frequencies. However, at fields greater than about 200 Gauss, most of the energy levels overlap. This makes quantitative analysis difficult at the fields used in this study.

3.5 C-4

The principal component of the "plastic explosive" C-4 is RDX. RDX has two inequivalent nitrogen sites and, therefore, two quadrupole coupling constants: 5.733 MHz with an asymmetry parameter of 0.622, and 5.731 MHz with an asymmetry parameter of 0.656 [1].

RDX exhibits four NQR frequencies, and there is little overlap of energy levels even at fields in excess of 1,000 Gauss. Unfortunately, the rf irradiation produced severe dielectric heating of the sample and, hence, rf pumping effects could not be explored in this compound. Instead, we studied the NMR free induction decay (FID) of C-4 and, as a result, observed some interesting lineshape and relaxation behavior.

3.6 Predictions

As discussed in Appendix A, attempts were made to predict the frequencies of the off-resonance transitions for HMT. However, the results of these

attempts were not satisfying. In part, this was because the nitrogen Larmor frequency was near the nitrogen NQR frequency and, in part, because HMT (and the other compounds studied) were polycrystalline. No attempts were made to predict the frequencies of the off-resonance transitions for the explosive compounds, since these had the added complication of non-zero asymmetry parameters.

4 Laboratory Methods

The laboratory methods and equipment used to acquire NMR signals and the off-resonance rf pumping data are fully described in Chapter 3 of Appendix A. However, to acquire the data on the explosive compounds presented here, a new probe for the NMR spectrometer, which operates at 19.14 MHz, was designed and constructed.

There are two principal advantages to the new probe. First, the old probe contained a small amount of proton-containing material and this produced a small residual signal which had to be taken into account. The new probe was fabricated out of copper and Teflon only, and eliminated the residual signal problem. Second, the modified probe allowed for a more efficient sample coil design which produced a modest improvement in the signal-to-noise ratio of the system.

The samples of HMT and mannitol were obtained from the Aldrich Chemical Company. The samples of explosive compounds were obtained from the San Diego Fire Department and are assumed to be commercial grade.

5 Experimental Results

NMR data were taken on five separate compounds: one explosive simulant, hexamethylenctetramine (HMT); one benign compound, mannitol; and three explosive compounds. The three explosive compounds were PETN, TNT and C-4. The experimental results obtained for these five compounds are presented below.

5.1 HMT

The experimental results for HMT are shown in Figure 1. This is a plot of the percentage decrease in the proton NMR response versus the rf pumping frequency. The conditions under which these data were acquired are discussed in Appendix A, and this figure is virtually identical to the one presented on page A61.

Some of the data points in Figure 1 have very small uncertainties, the result of a large number of observations averaged together. For example, there are true zeroes at 22.7 MHz and 23.1 MHz, and non-zero responses in the regions near 16.7 MHz, 22.0 MHz and 23.8 MHz.

Off-resonance pumping of HMT was also attempted near the NQR frequency of 3.308 MHz. The results, which show no effect, are shown in Figure 2.

One reason for the null result near 3.308 MHz may be that the probe irradiation coil was very difficult to tune at low frequencies. As a result, the maximum field in the coil was reduced by about a factor of about four, compared to the field produced at the higher frequencies.

Several attempts were made to tune the probe at frequencies near the nitrogen Larmor frequency of 1.383 MHz. These attempts were unsuccessful and, therefore, it was impossible to acquire data in this frequency region. However, the lack of data in this region is probably not serious, since effects at the nitrogen Larmor frequency would be unlikely to lead to unique NMR signatures in the proton responses of these compounds.

5.2 MANNITOL

Present explosive detection methods are designed to discriminate between explosives, which have long T_1 times, and commonly-encountered benign compounds, which generally have much shorter T_1 times. Therefore, unique NMR signatures are only needed to distinguish benign compounds with long T_1 times.

Only one benign compound was studied in this work, in part, because of the difficulty in finding nitrogen-free solid compounds with long T_1 times at room temperature. The compound we chose was mannitol, a complex sugar often used to cut cocaine. Mannitol has a T_1 of 281 seconds at room temperature [3], very close to the value observed for RDX.

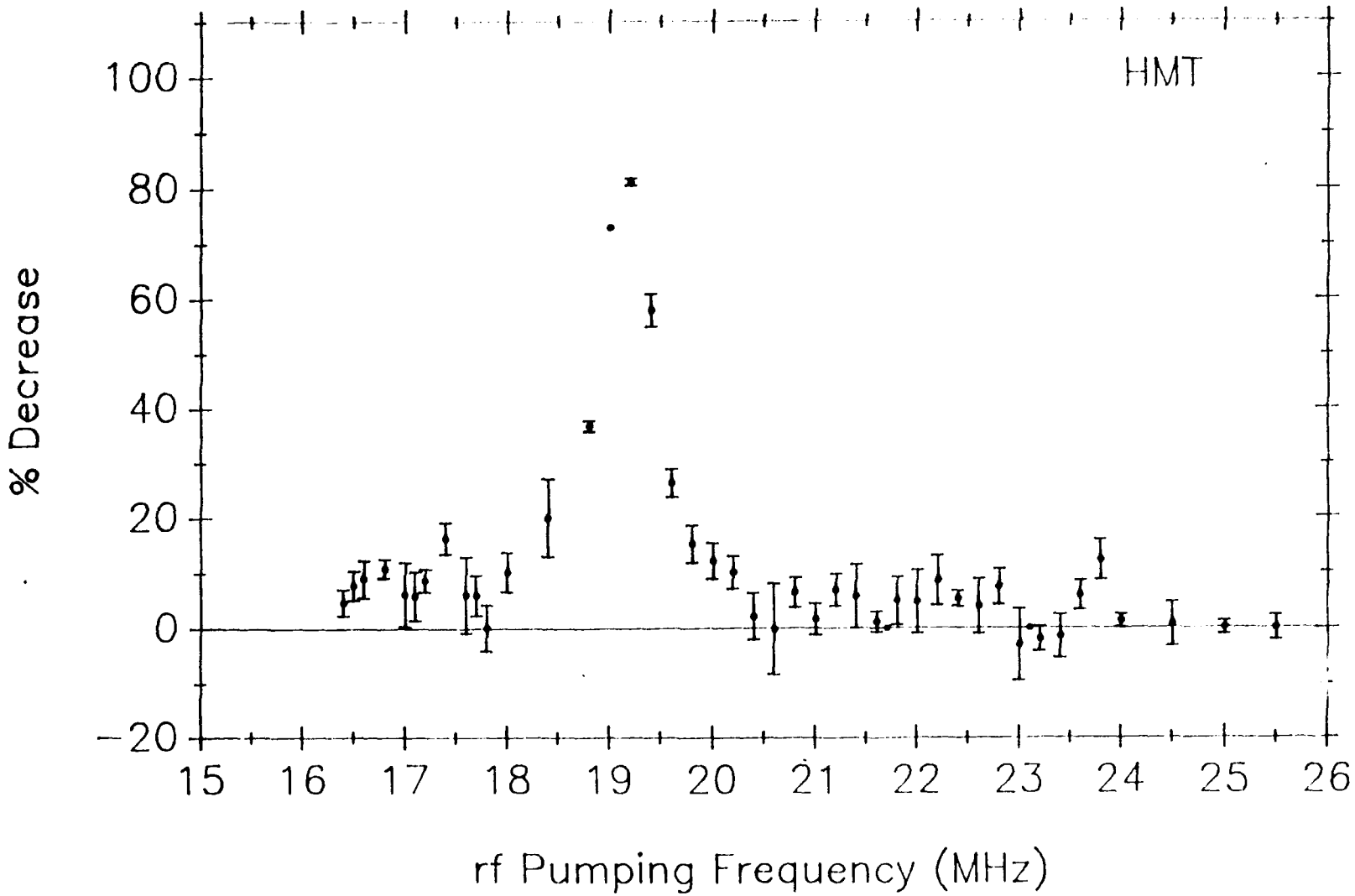
HMT
% Decrease
100
80
60
40
20
0
-20
15
16
17
18
19
20
21
22
23
24
25
26
rf Pumping Frequency (MHz)

Figure 1

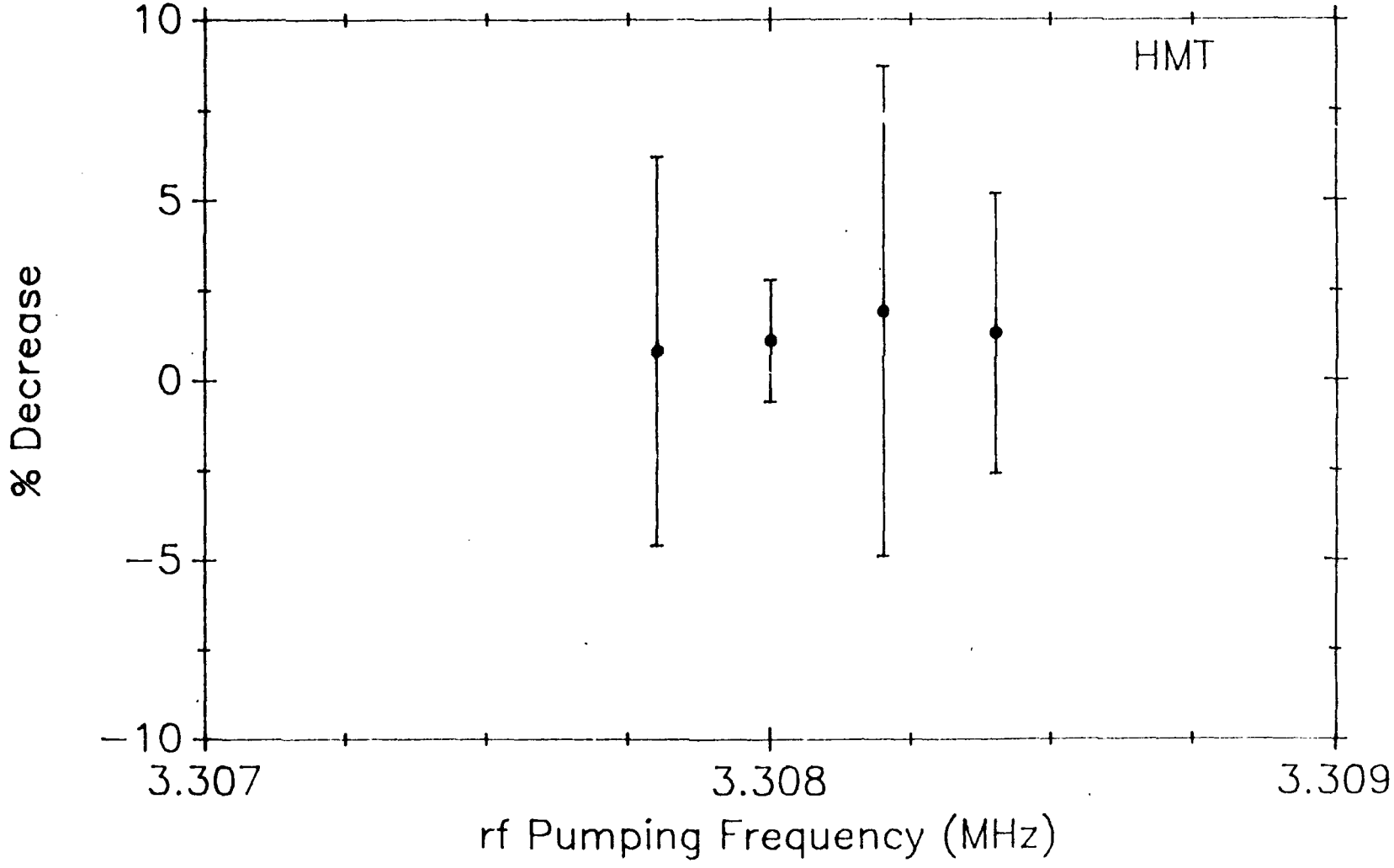
10
5
0
−5
−10
% Decrease
HMT
3.307
3.308
3.309
rf Pumping Frequency (MHz)

Figure 2

The data obtained from mannitol are shown in Figure 3, which is identical to that presented in Appendix A. The response to rf pumping near the Larmor frequency is due to the NMR linewidth, i.e., the short T_2. As expected from the lack of hydrogen-nitrogen interactions, no response to rf pumping was observed at frequencies significantly higher or lower than the Larmor frequency.

5.3 PETN

A plot of the percentage decrease in the proton NMR signal versus the rf pumping frequency for PETN is shown in Figure 4. It is clear from this figure that the effects of rf irradiation in PETN do not extend over as wide a range of frequencies as they do in HMT.

However, the structure of the response may be as complex as HMT. There is a pronounced effect at 20.2 MHz which is followed by an apparent zero in the response at 20.25 MHz. Similar behavior was observed on the low frequency side of the proton resonance.

In addition, there are clear non-zero responses near 17.8 MHz and 20.6 MHz. No effects in PETN were observed above 21 MHz or below 17 MHz.

The data in Figure 4 are consistent with a symmetric response about the proton Larmor frequency. No data were acquired for rf pumping near the PETN NQR frequencies because of the probe-tuning difficulties described in the section on HMT.

5.4 TNT

The data obtained for TNT are shown in Figure 5. There is little or no response far from the proton Larmor frequency, though there appear to be small effects starting about a one megahertz away from resonance, i.e., in the 20 - 21 MHz region.

The most striking feature of the data of Figure 5 is that the response appears to be asymmetric about the proton Larmor frequency of 19.14 MHz. At one-half megahertz above the proton Larmor frequency, the effect of rf pumping on the proton signal is still significant, i.e., between five and ten percent. On the other hand, one-half megahertz below the proton Larmor frequency, the response is clearly zero. Determination of the asymmetry of the response to pumping is well outside the range of experimental uncertainty.

Again, no data were acquired for rf pumping near the TNT NQR frequencies because of the probe-tuning difficulties described in the section on HMT.

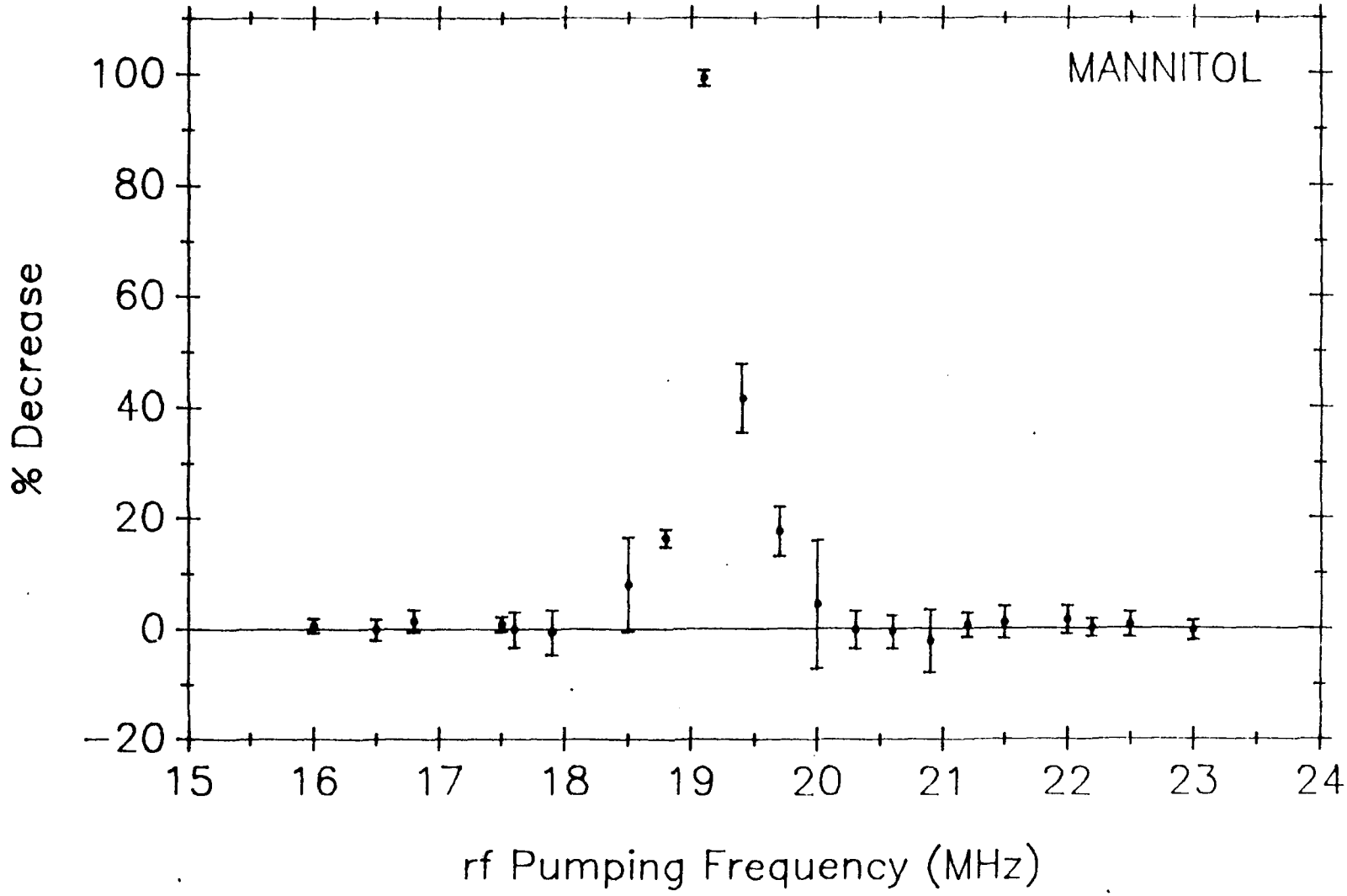
MANNITOL
% Decrease
100
80
60
40
20
0
-20
15
16
17
18
19
20
21
22
23
24
rf Pumping Frequency (MHz)

Figure 3

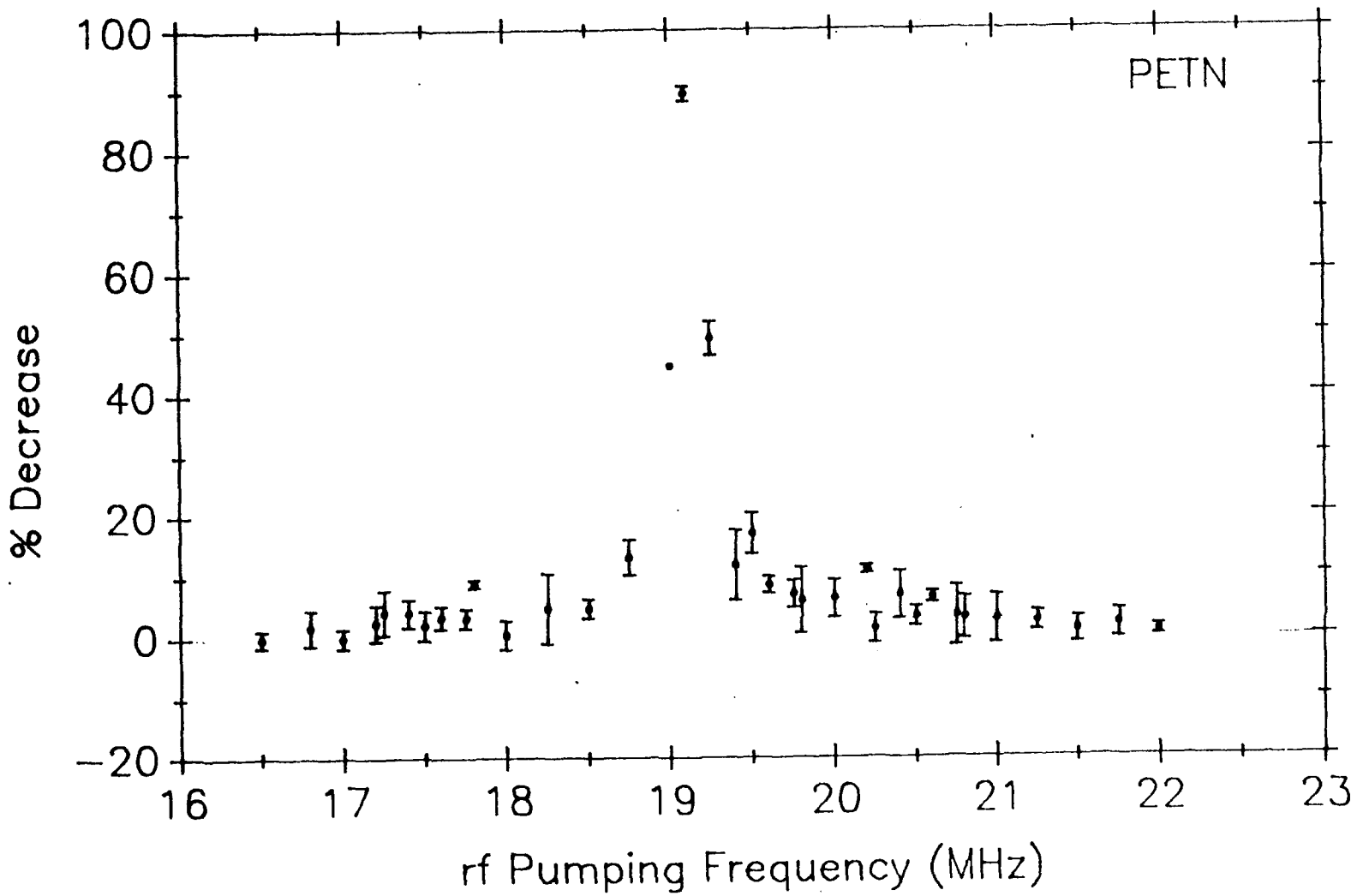
PETN
100
80
60
40
20
0
-20
% Decrease
16
17
18
19
20
21
22
23
rf Pumping Frequency (MHz)

Figure 4

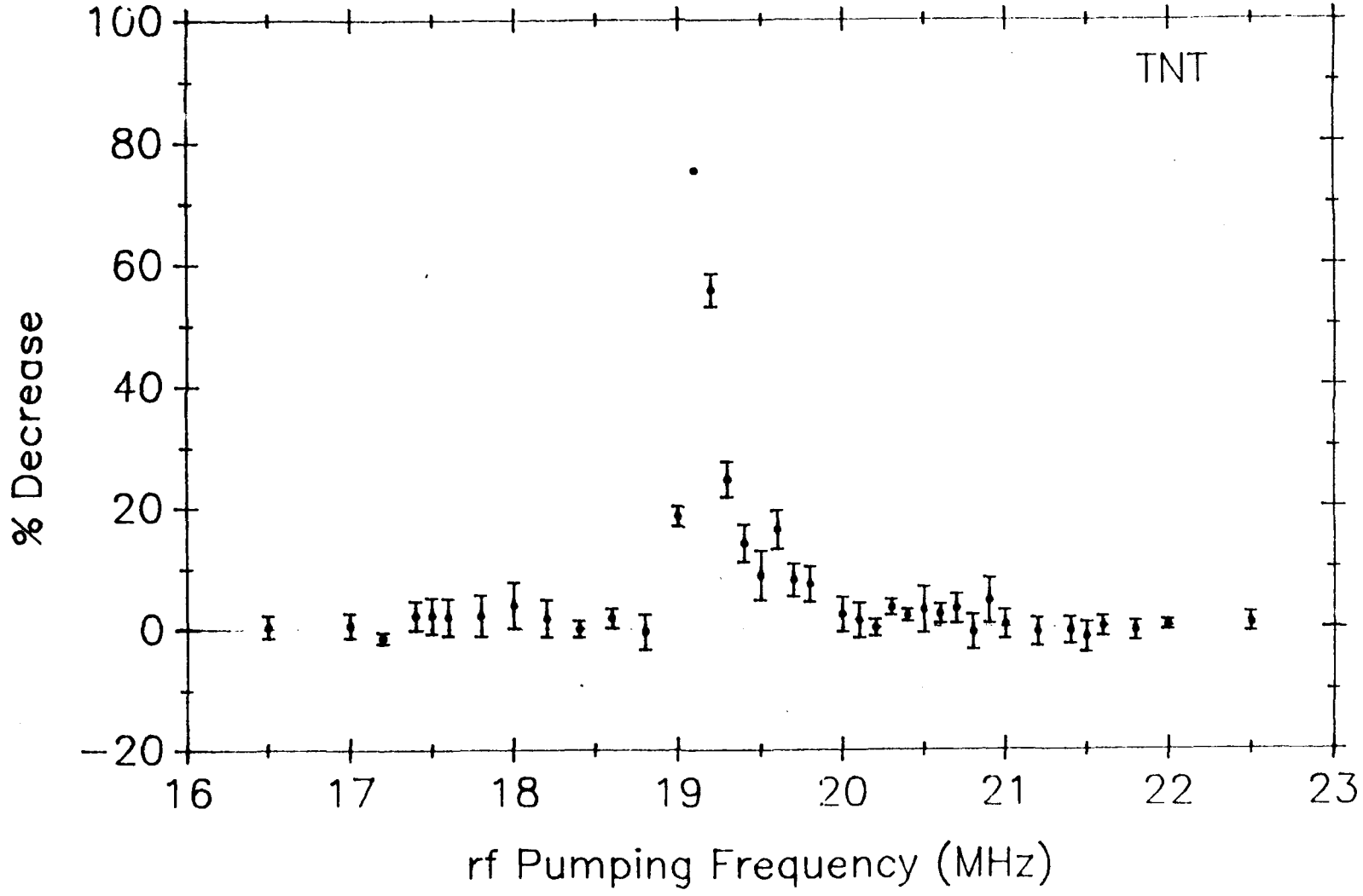
100
80
60
40
20
0
-20
% Decrease
TNT
16
17
18
19
20
21
22
23
rf Pumping Frequency (MHz)

Figure 5

5.5 C-4

Experiments similar to those carried out on the compounds above were started on the "plastic" explosive C-4, but the rf irradiation caused dielectric heating and the sample became very warm. In fact, the sample turned from snowy white to a very dark brown and, as a result, the rf pumping experiments were discontinued.

As an alternative, we studied the C-4 NMR free induction decay (FID). Previous studies have concentrated on RDX, the principal explosive component of C-4. Our observations indicate that there are significant differences between the NMR properties of RDX, which has a single short T_2, and C-4.

The FID of C-4 contains two components. One component has a long T_2, similar to T_2's frequently observed for viscous liquids. The other component has a short T_2, with characteristics similar to those observed for other explosives.

The long T_2 component from our C-4 sample is shown in Figure 6. It is likely that this component of the signal is due to some of the minor constituents of C-4 such as motor oil and polyisobutylene. For clarity, the beat pattern was produced by shifting the magnetic field slightly to move the Larmor frequency away from the spectrometer frequency.

The horizontal scale of the trace in Figure 6 is two milliseconds per division and the vertical scale is 0.5 volts per division. The T_2^* for this component of the NMR FID is approximately 4.5 milliseconds, while T_1 is about 100 milliseconds.

The short T_2 component of the C-4 signal is shown in Figure 7 and is due, in large part, to the presence of RDX. This trace was taken immediately after the sample was immersed in the magnetic field. Therefore, the signal magnitude is due entirely to polarization at the highest level crossing field for RDX, approximately 1,110 Gauss [1].

The horizontal scale of the trace of Figure 7 is 10 microseconds per division and the vertical scale is 0.1 volts per division. The spectrometer gain setting is identical to that used in Figure 6. The T_2 for this component of the signal is approximately 7 microseconds.

The short T_2 component of the C-4 FID possesses a very long T_1. This is illustrated by the FID traces shown in Figures 8 and 9, which were taken at the same horizontal and vertical scales and gain setting used for Figure 7.

The FID shown in Figure 8 was taken after the sample was immersed in the field for five minutes. The FID magnitude is about twice that shown in Figure 7. The FID of Figure 9 was taken 10 minutes after immersion. This corresponds to approximately twice the C-4 T_1 of 280 seconds in this field.

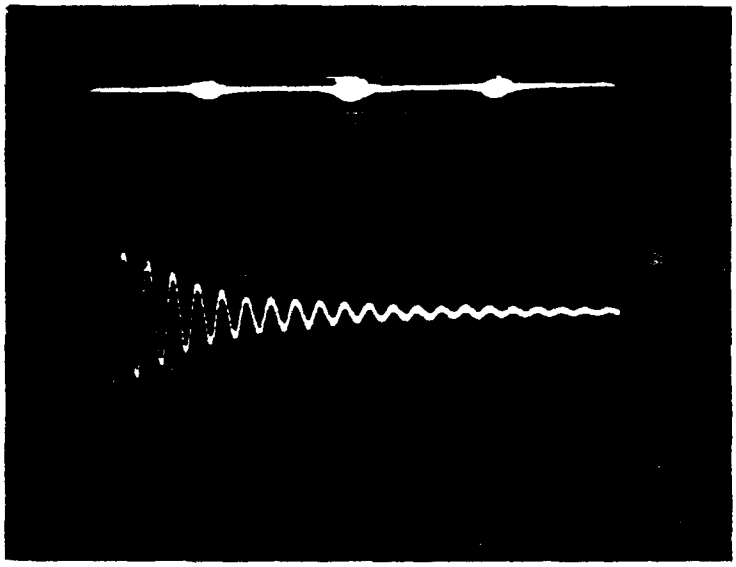

Figure 6

C-4 FID, Long T_2 Component

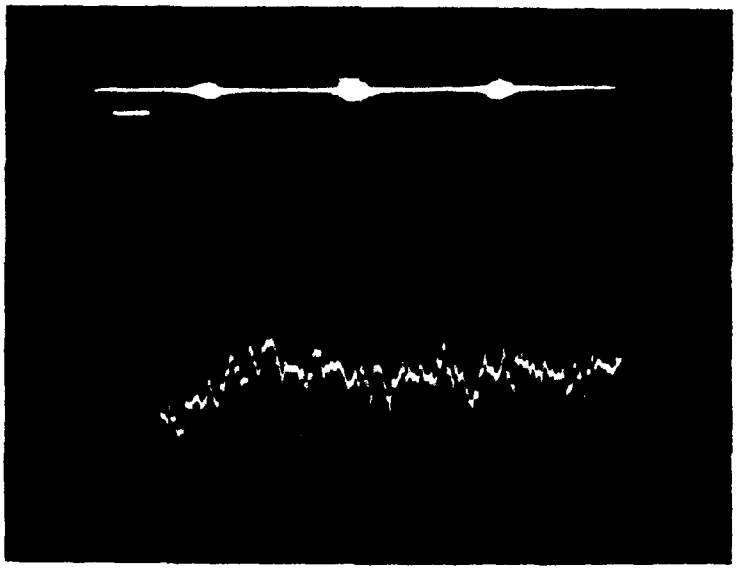

Figure 7

C-4 FID, Short T_2 Component

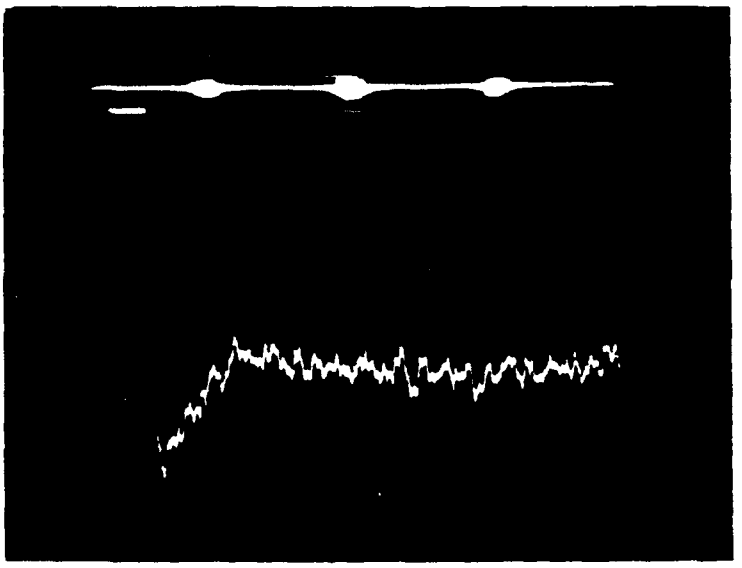

Figure 8

C-4 FID, After Five Minutes

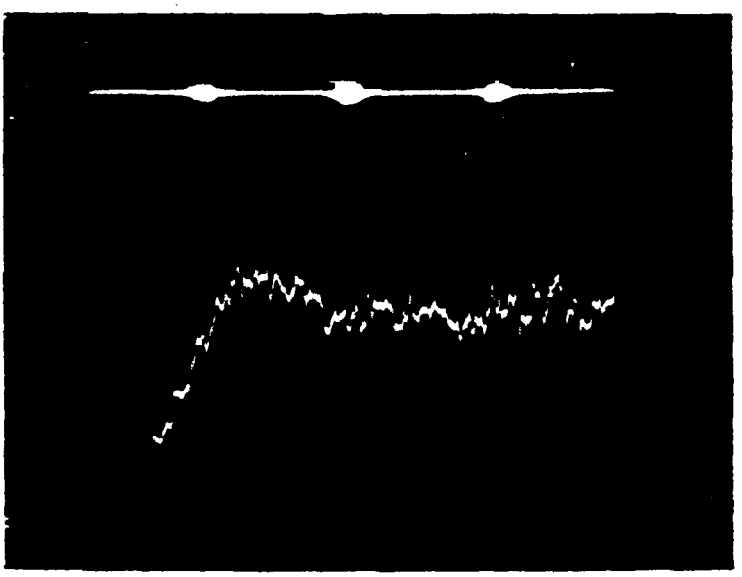

Figure 9

C-4 FID, After Ten Minutes

5.6 Signatures

Significant differences in the proton NMR responses were observed for the four compounds HMT, TNT, PETN and mannitol. In principle, using the pulse sequences of Appendix A, it would be fairly straightforward to design an instrument capable of distinguishing, with a fair degree of confidence, between the three nitrogen-containing compounds and mannitol. With additional sophistication, it would also be possible to determine which of the three nitrogen-containing compounds was under observation.

However, the observed differences are not large and, to be detectable in a field instrument, would require a considerable investment in hardware and a significant increase in observation time over present methods. In addition, the response of C-4 suggests that this approach should be used with caution.

The data in this study were taken for single-frequency irradiation and it is quite possible that alternative methods of rf pumping would yield larger effects and reduced observation times. In addition, since the data were taken at discrete frequencies, it is possible that significant effects occurring in narrow frequency bands were overlooked. However, we feel that this is unlikely.

References

1 J.D. King, W.L. Rollwitz and G.A. Matzkanin, "Nuclear Magnetic Resonance Techniques for Explosives Detection", Final Report, Parts I and II, US Army Contract No. DAAK02-74-C-0056, June 1975.

2 Lowell J. Burnett and Morton A. Fineman, "Evaluation of One-Sided Nuclear Magnetic Resonance for Remote Detection of Explosives", Final Report to the US Federal Aviation Administration, Contract No. N66001-87-D-0136, D.O. No. 0001, May 1988.

3 Lowell J. Burnett, "A Study To Evaluate Nuclear Magnetic Resonance for Narcotics Detection", Final Report on US Customs Order No. CS-085-2075-1, April 1986.

APPENDIX A

OFF RESONANCE PUMPING EFFECTS IN THE NMR OF SOLIDS

A Thesis

Presented to the

Faculty of

San Diego State University

In Partial Fulfillment

of the Requirements for the Degree

Master of Science

in

Physics

---

by

John Patrick Sanders

Spring 1988

OFF RESONANCE PUMPING EFFECTS IN THE NMR OF SOLIDS

A Thesis

Presented to the

Faculty of

San Diego State University

---

by

John Patrick Sanders

Spring 1988

Approved by:

Date 4/15/88

DEDICATION

This thesis, along with the past two years of work, is dedicated to

Morton A. Fineman.

ACKNOWLEDGEMENTS

I would like to thank Dr. Lowell Burnett for his continual support and praise of my work. I especially thank Dr. Burnett for taking the time to be much more than just a thesis advisor I saw once a week. Your patience and thoughtfulness are greatly appreciated.

I would also like to thank EG&G and the FAA for their financial support.

TABLE OF CONTENTS

LIST OF TABLES

LIST OF FIGURES

CHAPTER I

INTRODUCTION

The objective of the research reported in this thesis was to find a new technique for the detection of solid compounds that contain nitrogen. This is part of the general problem of detecting and identifying solid compounds through the use of nuclear magnetic resonance (NMR).

The basic idea of this research is to be able to differentiate between two classes of compounds. The first class consists of those compounds that contain nitrogen (that is, nitrogen-14), while the second class consists of those without. It may not be possible to identify the compound, though, once it has been determined whether or not any nitrogen is present. This aspect of solid detection is left for future studies.

The two compounds investigated, representing members of each class mentioned above, were hexemethylenetetramine (HMT) and mannitol. The first, HMT, contains four nitrogen atoms per molecule, while the second, the sugar mannitol, contains no nitrogen. These two compounds were chosen because they had relatively long proton spin-lattice relaxation times, i.e. approximately 60 seconds for HMT, and 280 seconds for mannitol at 19.14 MHz. These long spin-lattice relaxation times allowed for the development of a simple detection scheme since precise timing during the experiments was not essential.

The idea behind this research is a relatively simple one. Initially, we planned to irradiate the samples at the sum and difference of the nitrogen and proton Larmor frequencies and look for evidence of proton spin transitions. This irradiation should, in theory, cause transitions between the proton energy levels which would alter the rate of

return of the spin system to equilibrium following a disturbance. Since the system returns to equilibrium during the irradiation, the net effect is to lengthen the apparent spin-lattice relaxation time. This results from the fact that a fraction of the nuclei which have fallen back to equilibrium will be redistributed.

The main problem in this research was the acquisition of the data. To accomplish this an NMR probe had to fabricated so that we could first irradiate the sample, and then apply a 90° pulse so that the Free Induction Decay (FID) of the sample could be examined. Since the analysis is based upon these results, they had to be accurate.

The thesis is divided into three major sections. The first section deals with the basic aspects of NMR. However, not much time is spent on this aspect of the problem since there are many references (1,2,3) which deal with it in great detail. A topic that is completely overlooked is pulse NMR. This is because short, intense rf fields impressed upon the nuclear spin system produce complex effects that are difficult to characterize in a brief discussion. For an in-depth treatment of the subject, comprehensive references are readily available (4).

The second section is an overview of what transpired during the course of the experiment. This section is basically an account of the events, in chronological order, that led to the final probe design and experimental technique. Since a number of measurement systems were designed and constructed in an attempt to observe and quantify the effects of off-resonance pumping, this section is very important.

Finally, the experiment itself, and the results obtained are discussed. This section is the heart and soul of the thesis. It is these few pages that make all the long hours and tedious work worthwhile.

CHAPTER II

THEORY

Introduction

Nuclei can be thought of as behaving like tiny spinning particles. Since nuclei bear charge, their spinning produces a magnetic moment μ, a physical vector quantity. The strength and direction of the magnetic field surrounding the nucleus can be calculated from μ. The fields produced by these magnetic dipoles are similar to those of microscopic bar magnets.

When immersed in a static magnetic field, the randomly-oriented magnetic dipoles respond to the force of the field by trying to line up with it. For the proton, quantum mechanics specifies that there are two allowable states with orientations "parallel" to the field (spin up) and "antiparallel" (spin down) corresponding to low and high energy states, respectively. Actually, the spins do not align exactly with the magnetic field, but rather are tilted at an angle θ, and the magnetic dipoles therefore precess about the direction of the field.

The interaction energy of the nuclear dipole with the applied magnetic field is of amount $-\mu \cdot \mathbf{B}$ (5). Furthermore, the nuclear magnetic moment, $\mu = \gamma \mathbf{J}$, where $\mathbf{J}$ is the nuclear angular momentum, experiences a torque. The angular momentum, $\mathbf{J}$, may be written as $\hbar\mathbf{I}$ (6), where $\mathbf{I}$ is the spin angular momentum. Quantum mechanics requires that $\mathbf{I}$ have magnitude $[I(I + 1)]^{1/2}$ and that the only measurable values of this vector are given by the magnetic quantum number, m, which may take on the values I,I-1,...,-I. Each value of m corresponds to a particular orientation of the nuclear magnet in the

applied field. A nucleus may therefore occupy one of the 2I+1 orientations and the energies are given by (7)

$$E_m = -\mu \cdot \mathbf{B} = -B_0 m\gamma\hbar,$$

where γ is the gyromagnetic ratio, a fundamental physical constant for each nuclear species.

Since $\Delta E = \hbar\omega$, the relationship between ω_0, the Larmor frequency, and B_0 is found to be

$$\omega_0 = \gamma B_0. \qquad (1)$$

Equation (1) is referred to as the Larmor relationship.

In reality, no nucleus exists alone, and the NMR experiment would not be feasible without a collection of magnetic moments. The proton, because of its large abundance and favorable magnetic moment, lends itself best to NMR studies.

The phases of precessing magnetic moments of an ensemble are random, that is, the tips of the magnetic moment vectors have different locations on the precessional orbit. The individual spin vectors lie on the surface of a double cone and the vector sum of their alignments produces a macroscopic magnetization or magnetic moment **M**. It is this net magnetic moment which is responsible for the induction of the NMR signal in the receiver coil.

Magnetic resonance absorption can only be detected if transverse magnetization, that is, magnetization perpendicular to B_0, is established. It is the transverse component, M_{xy}, which is time-dependent and, according to Faraday's Law of Induction, can induce a voltage in the receiver coil. Transverse magnetization results whenever a small radiofrequency (rf) field of amplitude B_1, rotating synchronously with the precessing spins, is applied. When this rf field acts in a direction perpendicular to the main field, the effect is to spiral the magnetization away from its equilibrium state. Just as the

individual magnetic moments sense the force due to the external field, constraining them to precess, the macroscopic magnetization senses the presence of the rf field and precesses about it. If the duration of the B_1 field is such that the net magnetization is rotated by an angle of 90 degrees, it becomes transverse, that is, perpendicular to the static field. The above is the definition of a 90° pulse that will be referred too throughout this thesis.

Energy Absorption

Following a line of reasoning similar to that of Slichter (8), consider a system whose nuclei possess spin 1/2. There are many nuclei in a sample, but only two states for them to occupy as depicted in Figure 1. The number in the lower state is denoted by N_+ and those in the upper by N_-.

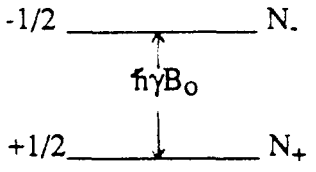

Figure 1. Energy levels for spin 1/2.

Slichter has shown that the transitions induced by the rf field yield the rate equation

$$\frac{dn}{dt} = -2Wn \qquad (2)$$

where $n = N_+ - N_-$, and W is the probability per second of inducing a transition by electromagnetic irradiation from +1/2 to -1/2, or vice versa.

The rate of energy absorption can be calculated from the above and is just

$$\frac{dE}{dt} = N_+W\hbar\omega - N_-W\hbar\omega = \hbar\omega Wn. \qquad (3)$$

If equations (2) and (3) described the system completely, the resonant absorption of energy would eventually stop and the resonance signal would disappear.

In the absence of a radiation field, the final equilibrium populations N_+^o and N_-^o are given by the Boltzmann distribution as

$$\frac{N_-^o}{N_+^o} = \exp\left(\frac{\Delta E}{kT}\right) = \exp\left(\frac{\gamma\hbar B_o}{kT}\right). \qquad (4)$$

Therefore, there must exist a mechanism for inducing transitions between N_+ and N_-, which arises through the coupling of the spins to some other system, i.e., the so-called "lattice". If we let W_+ denote the probability per second of inducing a transition upward in energy (from + to -), and W_- the reverse process due to this coupling, we have in the absence of an rf field

$$\frac{dN_+}{dt} = N_-W_- - N_+W_+. \qquad (5)$$

In the steady-state dN_+/dt is zero, therefore, from equation (5)

$$\frac{N_+^o}{N_-^o} = \frac{W_-}{W_+}. \qquad (6)$$

Substituting equation (4) into equation (6), the ratio of W_- to W_+ is

$$\frac{W_-}{W_+} = \exp\left(\frac{\gamma\hbar H_o}{kT}\right).$$

Now assume that the lattice has only two levels whose spacing is equal to that of the nuclear system. If the nucleus and the lattice are initially in the states of Figure 2 given

by the crosses, a possible transition is shown by the arrows. Note that in this transition conservation of energy is satisfied, as it must be.

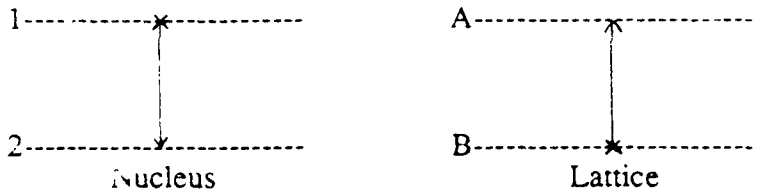

Figure 2. An allowed transition.

The nucleus, therefore, gives up its energy to the lattice. However, if both the nucleus and the lattice were in the upper states, no transition could occur since energy would not be conserved. From this example, it becomes clear that the probability that the reservoir is in a state which permits the transition must be a factor in the rate of transition of the nuclei.

By defining

$$n_0 = N\left(\frac{W_- - W_+}{W_- + W_+}\right)$$

and

$$\frac{1}{T_1} = W_- + W_+,$$

equation (5) may be rewritten as

$$\frac{dn}{dt} = \frac{n_0 - n}{T_1} \tag{7}$$

where n_0 represents the thermal equilibrium population difference and T_1 is a characteristic time associated with the approach to thermal equilibrium. Combining the

two rate equations, (equations (2) and (7)), to find the actual transition rate due to both thermal processes and transitions induced by the applied alternating field yields

$$\frac{dn}{dt} = -2Wn + \frac{n_o - n}{T_1}. \tag{8}$$

When a steady state is reached, the population difference is given by

$$n = \frac{n_o}{1 + 2WT_1}.$$

Spin-Lattice Relaxation

As mentioned in the last section, T_1, the spin-lattice relaxation time, is a characteristic time associated with the approach to thermal equilibrium. Relaxation times in NMR are influenced strongly by molecular motions which may alter the angles and/or distances between the nuclei. In many compounds, the rate and nature of molecular motions completely determines the spin-lattice relaxation time.

Following the discussion in a recent study (9), differences in the proton NMR relaxation properties of compounds form the basis for many detection methods, and it is likely that new NMR signatures based on the results of this work could be interpreted as changes in relaxation times in the presence of off-resonance irradiation. Therefore, a general appreciation of the reasons why different materials exhibit different NMR relaxation times is important.

In general, the spin-lattice relaxation time for protons is influenced by the strength of the magnetic interaction between a given proton and its neighbors and the relative motions between the proton and its neighbors. When the frequency of this relative motion is at, or very near, the Larmor frequency, then T_1 is short. The strength of the magnetic interaction depends primarily upon the nearest neighbor distances and the

strength of the neighboring moments. Because of their large magnetic moments, the presence of paramagnetic impurities has an extremely strong effect on the T_1's.

If the molecular motion near the Larmor frequency is simple, i.e., if there is only a single type of motion and all the nuclei participate, then the behavior of T_1 is relatively easy to characterize. The behavior of T_1 is usually expressed in terms of τ_c, the correlation time for the molecular motion. If, for example, the molecular motion is translational diffusion, then the correlation time can be thought of as the average time between diffusional jumps. If the motion is molecular reorientation, then the correlation time can be thought of as the average time it takes for a molecule to rotate through an angle of one radian. The correlation time may be thought of as roughly the average of the inverse of the frequency of molecular motion.

Figure 3 is a log-log plot of T_1 versus the correlation time for three different Larmor frequencies. In the region of short correlation times, i.e., for high temperatures in most substances, the frequency of molecular motion is much higher than the Larmor frequency. Here the T_1 of the material is long and increases as the correlation time decreases. Also, in this region, T_1 is independent of the Larmor frequency chosen.

When the frequency of molecular motion is roughly equal to the Larmor frequency, T_1 goes through a minimum. Since Larmor frequencies can be altered experimentally by changing the strength of the applied field, separate T_1 minima may be distinguished. These are shown in Figure 3.

When the correlation times are long, i.e., at low temperatures, where the frequency of molecular motion is low compared to the Larmor frequency, then T_1 is again long and lengthens with increasing correlation time. However, in contrast to the short correlation time region, the specific values of T_1 in this region depend upon the Larmor frequency employed for observation. Therefore, some indication of the nature of the

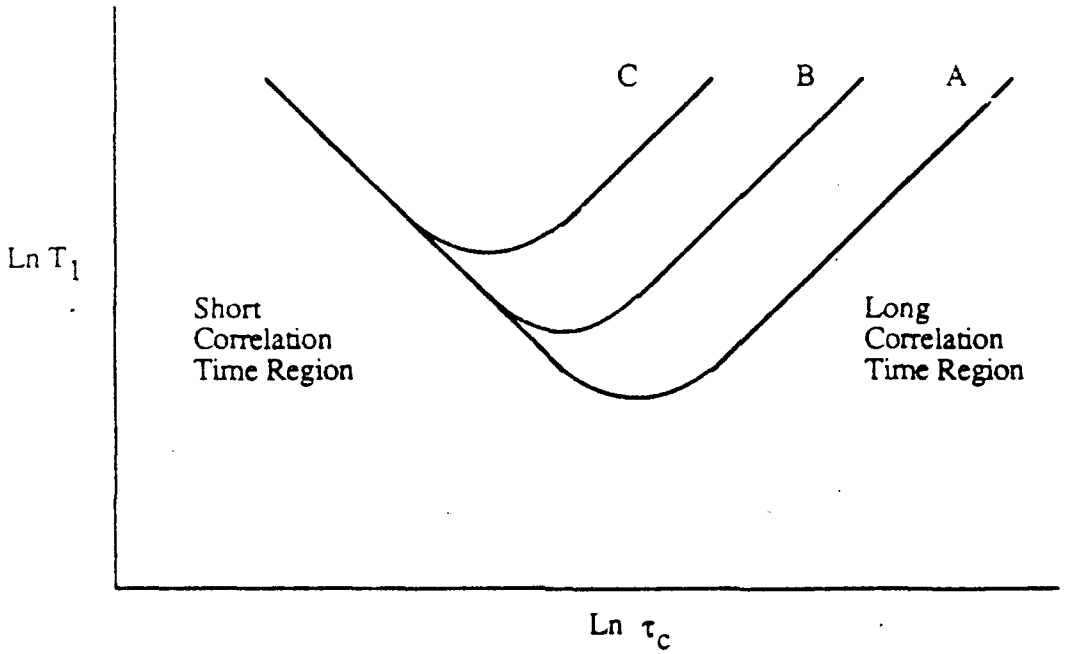

Figure 3. Spin-lattice relaxation time versus correlation time for molecular motion.

molecular motion can be obtained through studies of the Larmor frequency dependence of T_1 relaxation times.

Of all the possible molecular motions occuring in common substances, three often occur at rates close enough to the Larmor frequency to influence T_1. These three motions are molecular tumbling, molecular diffusion, and reorientation of mobile internal groups. One, or more, of these three motions generally determines the relaxation times.

In solids, molecular diffusion and tumbling usually proceed at rates slow compared to the Larmor frequency. Therefore, in rigid crystalline solids, such as those stated here, T_1 is generally long. In addition, since the atoms are fixed in place and the nuclei are essentially stationary, the couplings between nuclei are strong.

Furthermore, while most common organic substances possess side chains that are capable of internal motion, the compounds studied here are rigid. Therefore, the observed T_1's for the solid compounds investigated in this study are very long.

Nuclei with spin one ($I = 1$) are influenced by similar magnetic interactions with neighbors as spin one-half ($I = 1/2$) nuclei. Therefore, the spin-lattice relaxation time for spin one nuclei are influenced by the same molecular motions as discussed above. However, there is a major difference between nuclei with $I \geq 1$ and nuclei with $I = 1/2$. Nuclei with $I \geq 1$ possess a quadrupole moment, since they are not spherically symmetric, and this quadrupole moment interacts with the electric field gradients at the sites of the nuclei. The interaction energy between the quadrupole moment and the electric field gradient is generally much stronger than the interaction energy between the magnetic dipole moment and the applied magnetic field. Therefore, for nuclei with $I \geq 1$, relaxation effects due to the quadrupole interaction often dominate.

The strong interaction between nuclear quadrupole moments and electric field gradients produces relaxation times much shorter than those resulting from dipolar interactions between neighboring nuclei. For nitrogen nuclei in solids, T_1's in the range of 1 - 1,000 milliseconds are frequently observed, while for protons in similar molecules T_1's are often in the range of 1 - 100 seconds (10).

In zero applied field, and in weak fields, the nuclei align along the internal electric field gradients. However, when a very strong external magnetic field is applied, the nuclei align in the direction of the field. In general, the allowed energy levels for a particular nucleus depend upon the angle between the applied field and the symmery axis of the electric field gradient.

Since the electric field gradients in the molecule can point in any direction with respect to the externally applied magnetic field, there is often a broad range of interaction energies or allowed energy levels. Therefore, the resulting NMR response may be spread over a broad range of frequencies.

Strong and Weak Magnetic Fields

The allowed energy levels for nuclei with $I \geq 1$ depend upon the strength of the applied magnetic field. Thorough treatments of the theories for both the high and low field cases are found in both Abragam (11) and Slichter (12). Therefore, only a brief summary will be given here.

Assuming a field with axial symmetry (i.e., the asymmetry parameter $\eta=0$) we can illustrate the effective quadrupolar interaction. Consider the magnetic field to be applied along the z' axis and the electric field gradient symmetry axis along the z axis, where z' and z differ by an angle θ. Then, for a nucleus with spin I and electric quadrupole moment Q, the Hamiltonian is

$$H = -\gamma\hbar B_o I_{z'} + \frac{e^2qQ}{4I(2I - 1)}(3I_z^2 - I^2). \quad (9)$$

First consider what happens when the spins align along the magnetic field, i.e., the strong field case. If the x' axis lies in the plane containing z' and z,

$$I_z = I_{z'}\cos\theta + I_{x'}\sin\theta. \quad (10)$$

Substituting equation (10) into equation (9) yields

$$H = -\gamma\hbar B_o I_{z'} + \frac{e^2qQ}{4I(2I - 1)}[3I_{z'}^2\cos^2\theta + 3I_{x'}^2\sin^2\theta + 3(I_{z'}I_{x'} + I_{x'}I_{z'})\sin\theta\cos\theta - I^2].$$

Using quantum mechanics and collecting terms, the energy levels are found to be

$$E_m = -\gamma\hbar B_o m + \frac{e^2qQ}{4I(2I - 1)}\left(\frac{3\cos^2\theta - 1}{2}\right)[3m^2 - I(I + 1)]. \quad (11)$$

A contrasting experimental situation arises when the interaction energy (or coupling) due to the electric field gradient (efg) is larger than that due to the magnetic field (i.e., the spins align along the efg symmetry axis). Then it is appropriate to consider the quadrupole coupling as a first approximation. Using the same approach as above and including the Zeeman energy term it can be seen that the Hamiltonian is given by

$$H = -\gamma\hbar B_o m\cos\theta + \frac{e^2qQ}{4I(2I - 1)}(3I_z^2 - I^2). \quad (12)$$

From the Hamiltonian we see that the energy levels are

$$E_m = -\gamma\hbar B_o m\cos\theta + \frac{e^2qQ}{4I(2I - 1)}[3m^2 - I(I + 1)]. \quad (13)$$

Energy Level Diagrams

Employing the equations of the previous section, the energy levels can be easily calculated and the energy level diagrams drawn for a variety of cases. These range from no applied field and quadrupole effects only, to something as complicated as the

interaction energy of the applied field being approximately equal to the interaction energy of the electric field gradient.

When the applied magnetic field is zero, the interaction energy of the nuclear dipole moment with the field is zero. In this case, the internal electric field gradients align the nuclei and it is possible to provoke an NMR-like response with an rf field. This is called nuclear quadrupole resonance (NQR). Two excellent references on this subject are Lucken (13) and Dehmelt (14).

For the case of no applied magnetic field, equation (13) reduces to

$$E_m = \frac{e^2qQ}{4I(2I - 1)}[3m^2 - I(I + 1)]. \qquad (14)$$

Since I = 1 for nitrogen, $E_m = \frac{e^2qQ}{4}(3m^2 - 2)$, and the degeneracy in the $m = \pm 1$ states, as depicted in Figure 4, becomes quite apparent.

Examining equation (14), the change in the energy between the $m = \pm 1$ state and the $m = 0$ state can be shown to be

$$\Delta E = \frac{3e^2qQ}{4}. \qquad (15)$$

Dividing equation (15) by Plank's constant (h) converts the change in energy to a frequency. This frequency is the NQR frequency and is denoted by ν_q. Although it might not be obvious, ν_q depends upon the magnitude of the nuclear quadrupole moment (eQ), and the strength of the internal field gradients (eq).

Suppose now that a very strong magnetic field is applied such that the effects of the quadrupolar interaction are negligible. In this case the governing equation is

$$E_m = -\gamma\hbar B_o m$$

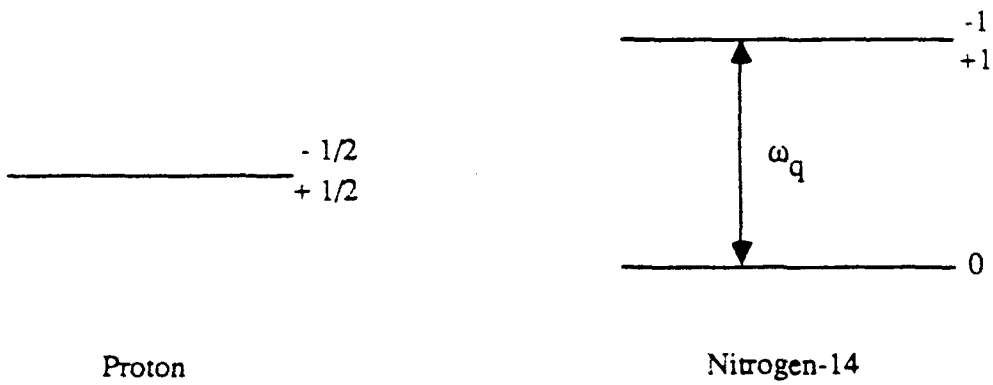

Figure 4. Proton and nitrogen energy levels in zero applied magnetic field.

where m can have any of the 2I + 1 values ranging from -I to I. This situation is depicted in Figure 5a for protons and Figure 5b for nitrogen. It is clear that the degeneracy is now removed.

When hydrogen and nitrogen nuclei are coupled together in a very strong magnetic field, there are six possible energy states for this system. Examining Figure 5c, it can be seen that there are 15 possible transitions for the proton + nitrogen coupled system. Notice that the $\Delta m = 2$ transitions for nitrogen have also been included. These overtone transitions were shown to occur by R. Tycho and S. J. Opella (15).

Of the 15 transitions shown in Figure 5c, seven occur at either the proton Larmor frequency (ω_p), or the nitrogen Larmor frequency (ω_n). At the magnetic field used in this study, these frequencies are 19.14 MHz and 1.38 MHz respectively.

The seven transitions that occur at ω_p or ω_n are allowed transitions, while the other eight transitions are forbidden. If these 15 states were pure, then the rate equations could be solved (16) to yield the probability that the particular transition is taking place. However, as pointed out by Abragam (17) and by Wind and Yannoni (18), these states are not pure states in solids. Each state is actually a mixture of all the possible states. The reason for this mixture of states is that the dipole-dipole coupling terms, which average to zero in liquids due to the rapid relative motion of the nuclei, do not average to zero in solids.

The states of Figure 5c then, are an admixture of states. Therfore, the eight forbidden transitions, i.e., for the pure states, actually become weakly-allowed. That is to say, the probability of a transition taking place is small, but it is non-zero.

For the protons there is no splitting due to quadrupole effects since I = 1/2; however, there is the common Zeeman splitting given by $\Delta E = \gamma\hbar B_0$. The nitrogen

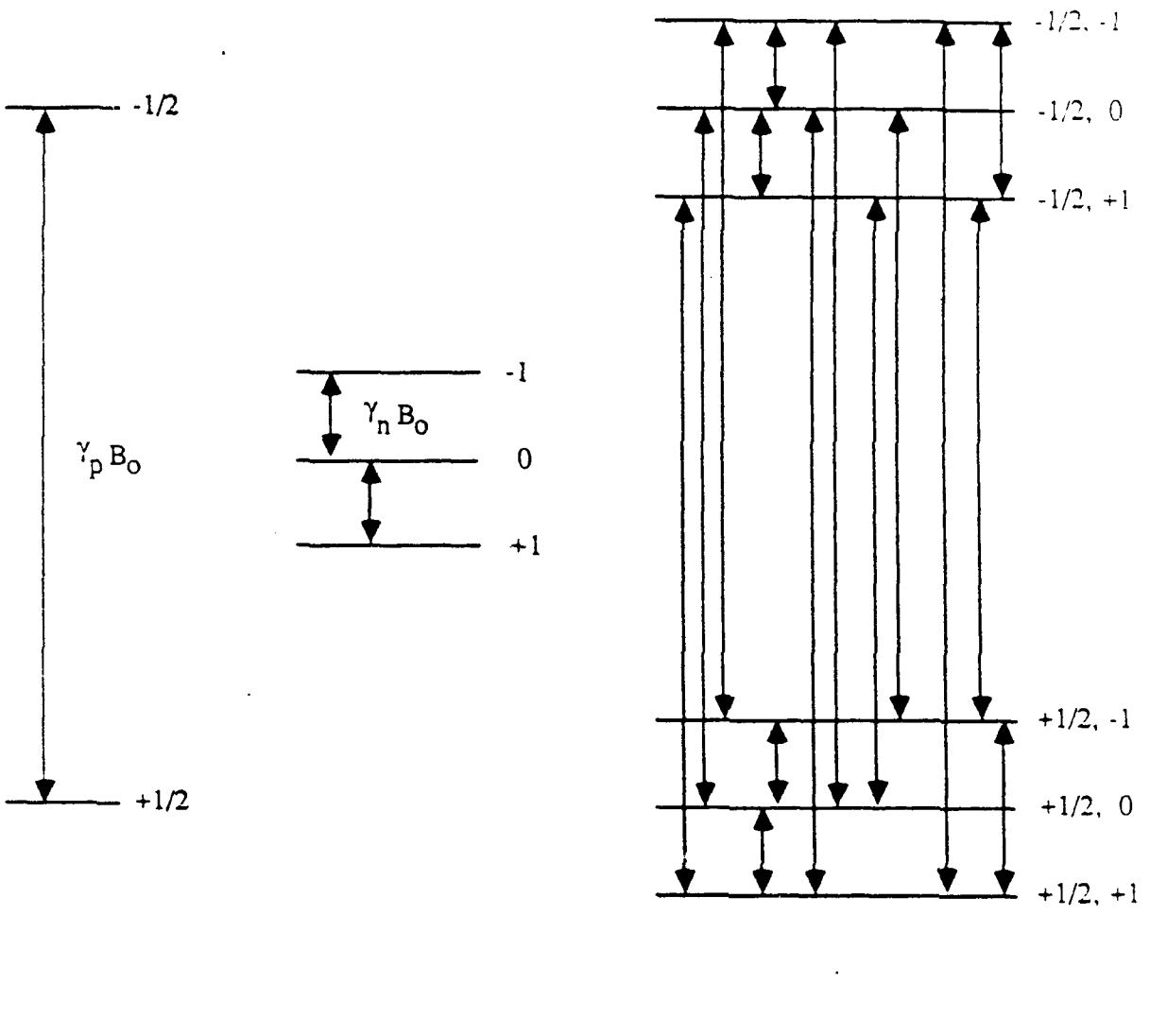

Figure 5. Energy levels for isolated proton and nitrogen, and for coupled proton and nitrogen nuclei; quadrupole effects ignored.

splitting is a bit more complicated when a low magnetic field is applied. For this case we must look at equation (13). Since I = 1 we have

$$E_m = -\gamma\hbar B_o m\cos\theta + \frac{e^2qQ}{4}(3m^2 - 2).$$

The energy level diagram for a compound containing both hydrogen and nitrogen is shown, in Figure 6, for a low field where the orientation of the electric field gradient symmetry axis with respect to the applied magnetic field is fixed. The splitting of the proton levels allows a single transition at the proton Larmor frequency. The applied field also splits the nitrogen $m = \pm 1$ levels, and the splitting depends upon θ, which is the angle between the applied field and the preferred alignment of the nitrogen nuclei along the internal electric field gradient symmetry axis.

Most solid samples studied by NMR are not single crystals, but are instead polycrystalline. Therefore, it is important to understand what happens to the energy levels in the situation where θ can have multiple values. The energy levels for a polycrystal in a low field with quadrupole effects included is shown in Figure 7. In a low field, the energy level diagram for a polycrystalline material is just a simple extension of Figure 6. The major difference is that in this case the angle θ is not unique and there is a continuum of levels extending from θ=0° to θ=180°.

The applied magnetic field can be adjusted to any value. Therefore, in principle, it is possible to investigate the case where the energy associated with the magnetic field is several orders of magnitude greater than the energy associated with the electric field gradient. Since the Zeeman magnetic field is larger than that associated with the electric field gradient, equation (11), which applies in this case, would consist of a dominant Zeeman term plus a quadrupole term that is a small pertubation. This pertubation term would result in a shifting of the energy levels of the nitrogen as depicted in Figure 8.

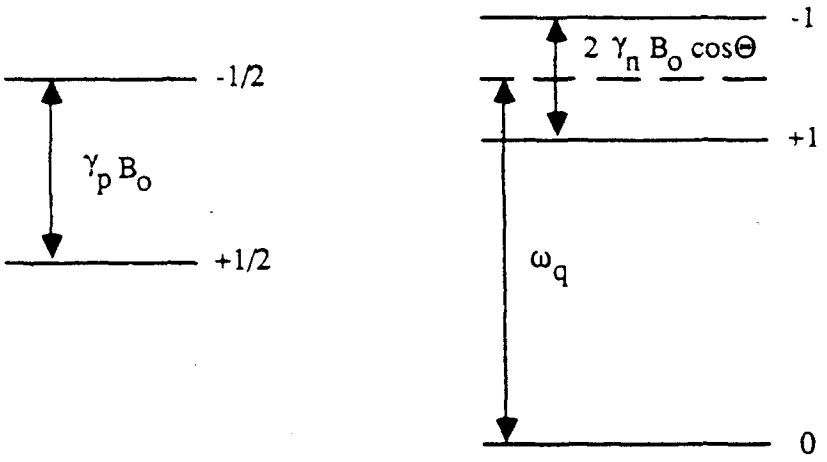

Figure 6. Proton and nitrogen energy levels; low field case; single crystal material, quadrupole effects included.

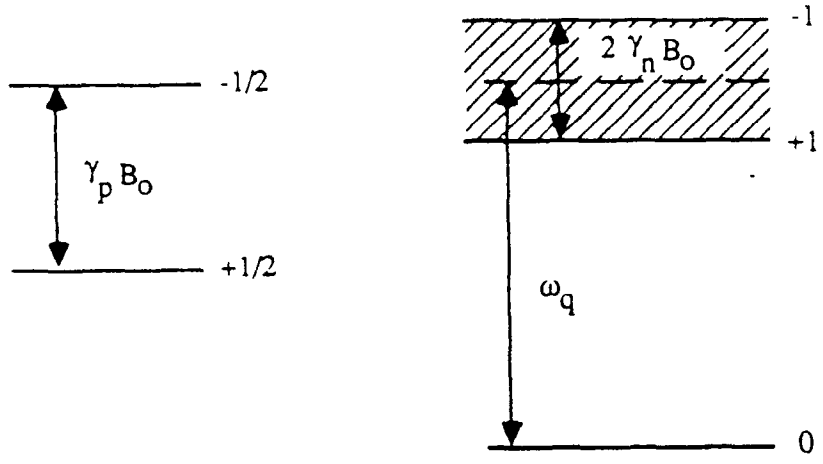

Figure 7. Proton and nitrogen energy levels; low field case; polycrysralline material, quadrupole effects included.

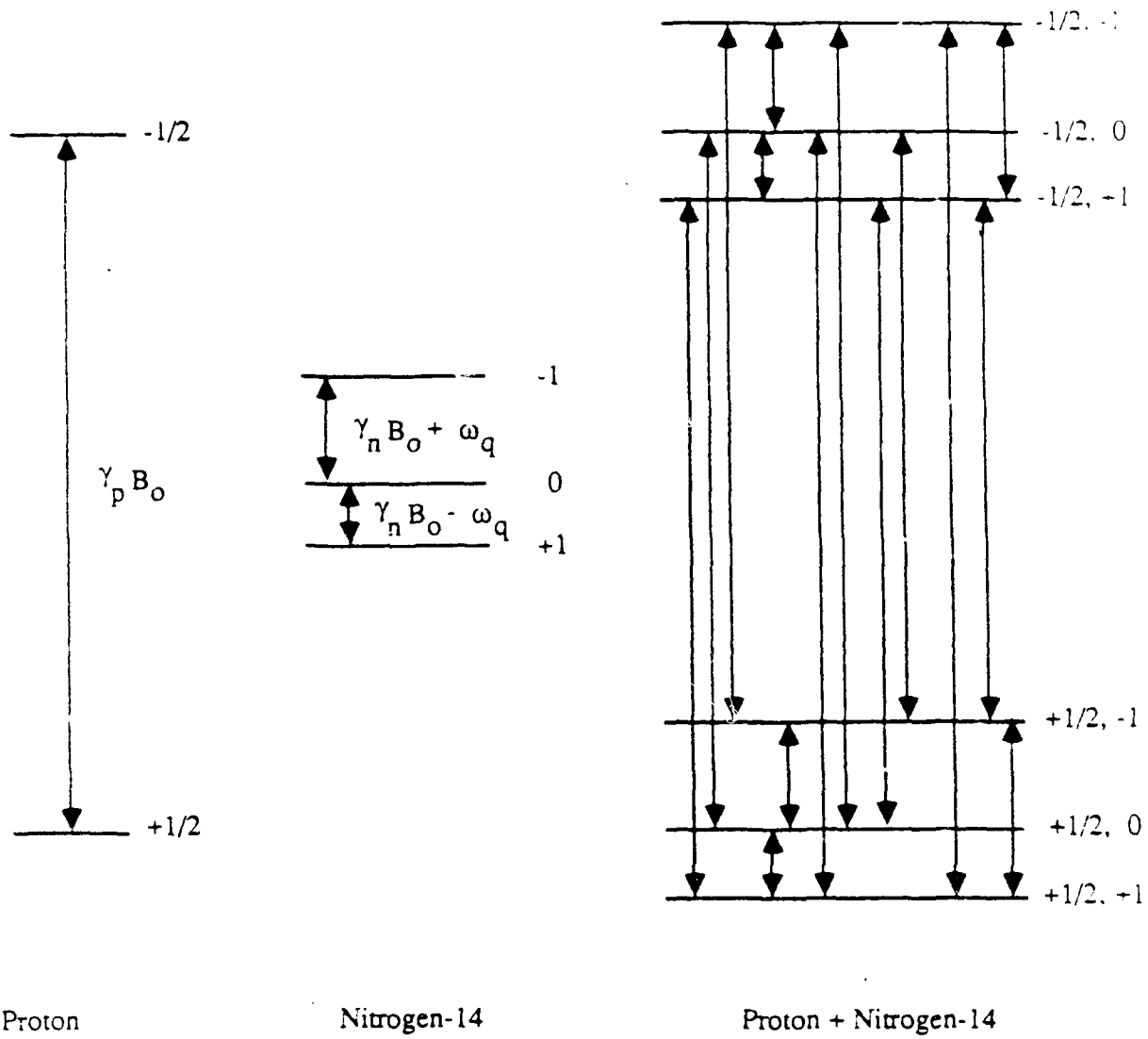

Figure 8. Energy levels for proton, nitrogen, and coupled proton and nitrogen nuclei; high field case, quadrupole effects included.

There are two important things that must be noted about Figure 8, though. First, the shifting shown in the figure is not drawn to scale. This should be clear from the above discussion, since one term is a small pertubation to the other. Second, and most important, the energy level diagram for Figure 8 is for one particular angle. This can be understood from a closer inspection of equation (11). Here again the fact that I=1 for nitrogen will be used to yield

$$E_m = -\gamma\hbar B_o m + \frac{e^2qQ}{8}(3\cos^2\theta - 1)(3m^2 - 2) \qquad (16)$$

Since θ is the angle between the electric field gradient symmetry axis and the applied magnetic field, equation (16) will have a continuous range of energy levels depending on the angle θ. This presents an interesting problem when the intermediate case is considered in detail.

The most interesting and difficult case, and the one that applies for our experiments, is that of the intermediate field. When the term "intermediate field" is used, it implies that the Zeeman energy is comparable to the quadrupole energy. The difficulty with this region, though, is that there is no theory to describe what should happen. Thus, only educated guesses can be made as to what is happening. Hopefully, the two extreme cases (i.e., low and high magnetic fields) together with the experimental results obtained herein will make some sort of theoretical interpretation possible.

The problem that the intermediate case poses is easy to understand. To obtain the eigenstates and the eigenvalues for the intermediate case, it would be necessary to solve a secular equation of order 2I+1, and that is already of third order for the smallest spin possessing a quadrupole moment: I=1 (19). Because the Hamiltonian equation has not been solved in this region of magnetic field, this region will be investigated examining the results of the accepted theories for the high and low field cases. The primary

assumption, then, is that the results for the intermediate field can be approximated by assuming that the nuclei align along the magnetic field (high field case), or that they align along the electric field symmetry axis (low field case).

Since there is some simplicity in attacking the problem from the low field region, it will be investigated first. In this case, as seen from equation (13), there is a simple splitting of the energy levels due to the Zeeman contribution. However, since the applied magnetic field energy is a bit lower than the quadrupole energy, the levels are split as shown in Figure 9. If the material is polycrystalline, the energy levels are then spread over the region from m=+1 to m=-1, as indicated in the figure. This spreading of the energy levels is due to the fact that θ can have any value between 0° and 180°.

Approximating the intermediate case by use of the high field case is much more complicated than the above. This complication arises from the $\cos^2\theta$ term in equation (11). This dependence shifts all of the energy levels by some amount. The major difference, then, between this case and that of the low field approximation case is that the m = 0 level is no longer stationary. As illustrated in Table 1, the shifting of the energy levels is quite broad. Although θ can have any value between 0° and 180°, there is clearly symmetry between the values of $0° \leq \theta \leq 90°$ and $90° \leq \theta \leq 180°$.

Figure 10a is a representation of the case where the interaction energy of the applied field is much greater than the quadrupole energy. Figure 10b illustrates the data contained in Table 1. Note that α, β, and γ refer to the m equal 0, 1, and -1 states, respectively.

Finally Figure 11 shows the dramatic shifting of the energy levels due to the $\cos^2\theta$ dependence. Notice that the m = 0 state begins as the highest energy state, but ends up as the lowest energy state when $\theta = 90°$. There are also two angles where a degeneracy

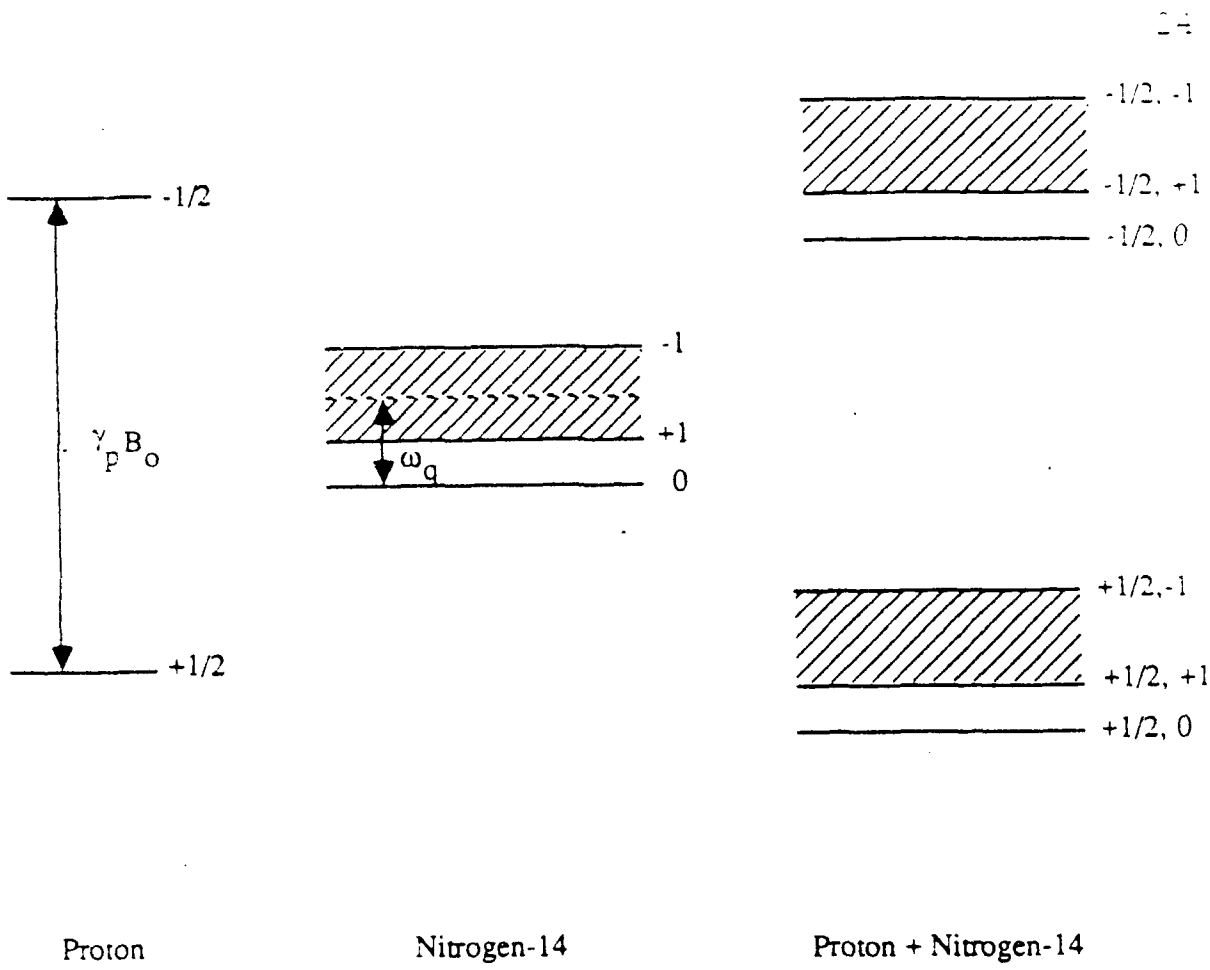

Figure 9. Proton and nitrogen energy levels; intermediate field case; polycrystalline material.

Table 1. Energy levels calculated from equation (15)

Angle	m	Energy (MHz)
0°	0	-2.205
	1	-0.280
	-1	2.486
15°	0	-1.984
	1	-0.391
	-1	2.375
30°	0	-1.378
	1	-0.694
	-1	2.072
45°	0	-0.551
	1	-1.107
	-1	1.659
60°	0	0.276
	1	-1.521
	-1	1.245
75°	0	0.881
	1	-1.824
	-1	0.942
90°	0	1.103
	1	-1.934
	-1	.832

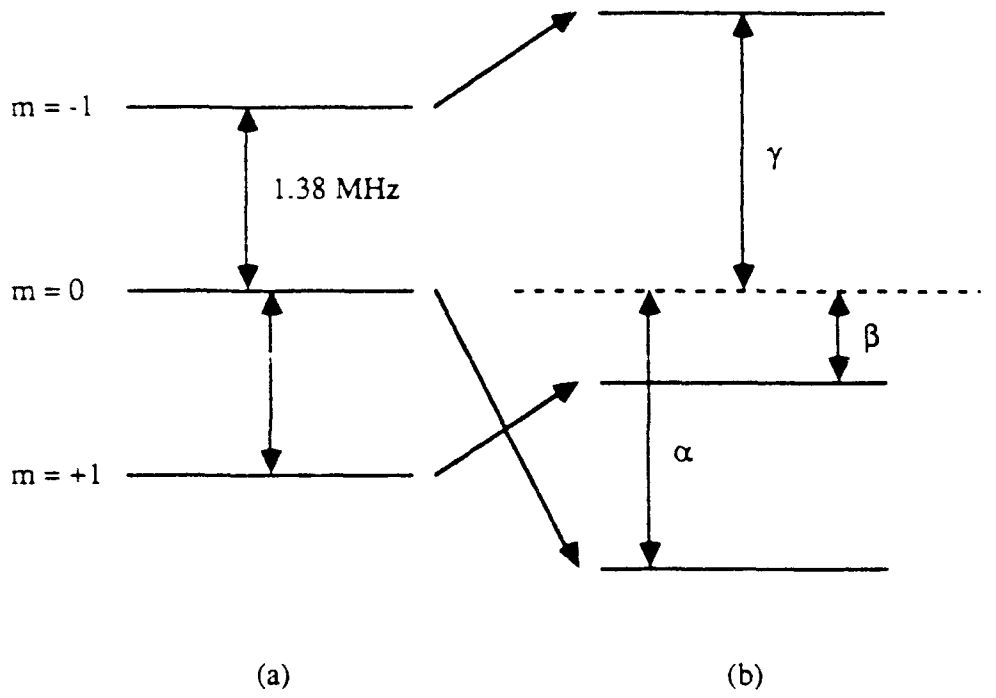

Figure 10. Shifting in the nitrogen energy levels due to the nuclei aligning along the applied magnetic field.

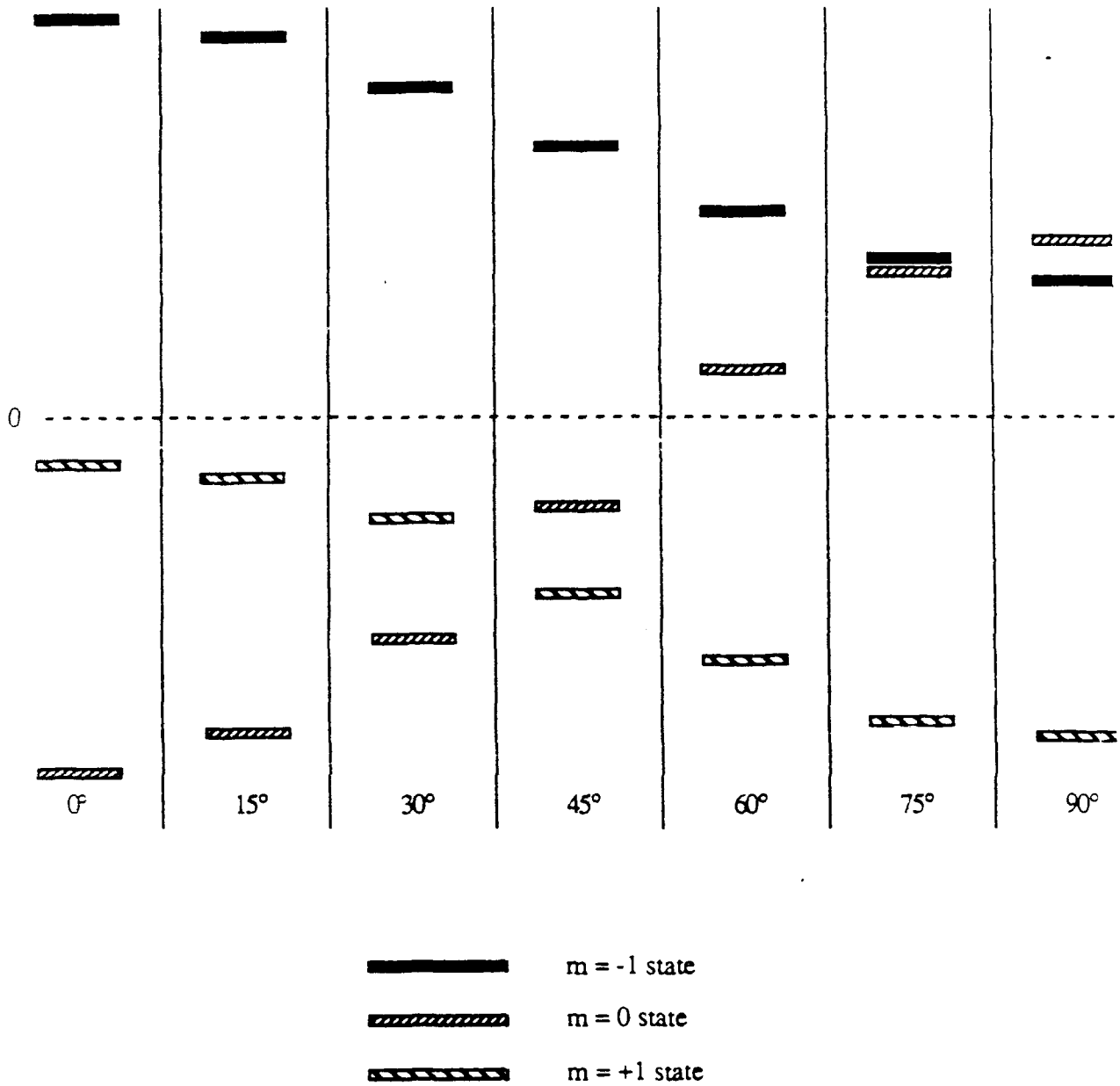

Figure 11. Theta dependence on the nitrogen for nuclei that align along the applied magnetic field. Only the m = +1/2 states of the hydrogen are shown.

is formed. The first degeneracy occurs at approximately $\theta = 38.5°$ where $E_0 = E_1$. The second degeneracy occurs when $E_0 = E_{-1}$, and takes place at approximately $\theta = 76.5°$.

CHAPTER III

EXPERIMENTAL DETAIL

Introduction

A number of different probes were designed and constructed in attempts to observe and quantify the effects of off-resonance pumping of weakly-allowed NMR transitions in nitrogen-containing compounds. These are detailed in this section following a discussion of a typical laboratory system for pulse NMR.

In addition, several different pulse sequences were tried in order enhance the effects of off-resonance pumping. These pulse sequences are also discussed in the following sections.

Typical Pulse NMR System

A block diagram of a typical laboratory pulse NMR system is shown in Figure 12. The magnet applies a static magnetic field to the sample while the radio frequency transmitter generates the rf pulses. The rf pulses are applied to the sample through the coupling network and sample coil.

The sample coil is also used to pick up the NMR free induction decay (FID) signal. Both the sample coil and the receiver are tuned to the Larmor frequency, and the receiver amplifies the weak FID signal prior to processing and display.

The controller is responsible for the circuit timing. It controls the duration of the pulses, the number of pulses in the test sequence, the timing of the data aquisition windows, and other similar tasks.

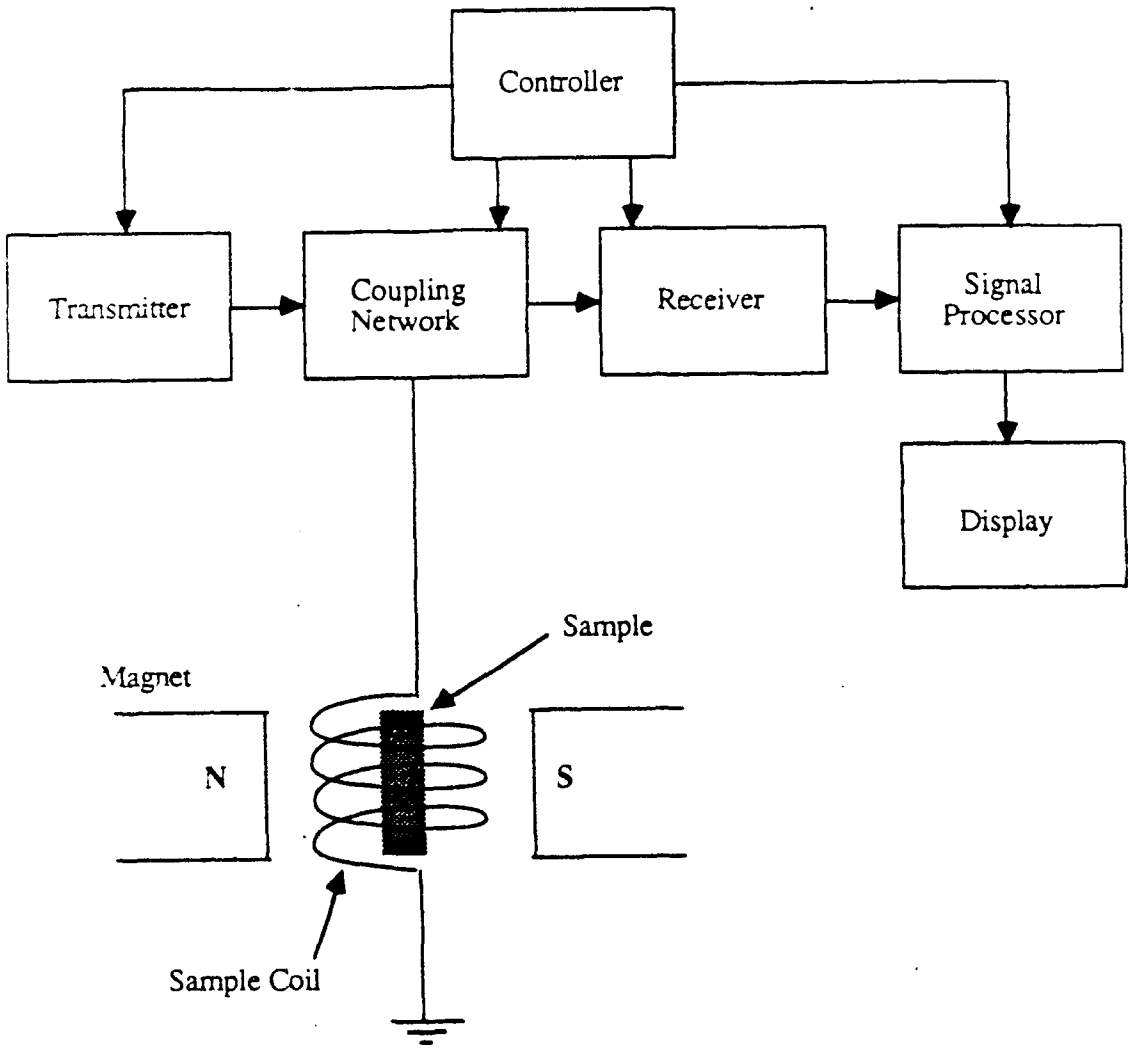

Figure 12. Block diagram of a pulse NMR system.

T_1 Measurements

Employing the above system, it is possible to measure spin-lattice relaxation times. Spin-lattice relaxation times are commonly measured in the laboratory with the two-pulse (180°-τ-90°) sequence shown in Figure 13. First, as shown in Figure 13a, a 180° pulse inverts the magnetization along the z' axis. Following the pulse, the nuclear magnetization begins to return toward its equilibrium value of M_0. After a time τ has elapsed, a 90° pulse is applied as depicted in Figure 13b. A free induction signal results, the initial height of which is proportional to the magnitude of **M**, hence the value of $M_{z'}$ at the time τ (20).

This experiment is repeated for a number of different pulse delay times τ. A plot of the FID magnitude versus τ provides the characteristic time for the return of the nuclear magnetization to equilibrium.

Pumping Techniques and Probes

During the course of this experiment both pulsed and continuous wave (CW) techniques were used to irradiate the sample and thus stimulate the weakly-allowed transitions. The advantages and disadvantages of each technique are discussed along with the probe designs that were employed. These discussions are presented in chronological order so that insight into the development of the final system can be gained.

A sketch of the first probe employed, the crossed-coil probe, is shown in Figure 14. A block diagram of a two-coil double irradiation system for pumping measurements is shown in Figure 15. It is clear from this diagram that separate coils are used for signal detection and for irradiating the sample, thus allowing the NMR spectrometer to always be connected to the sample coil. To keep the coupling of the sample and irradiation

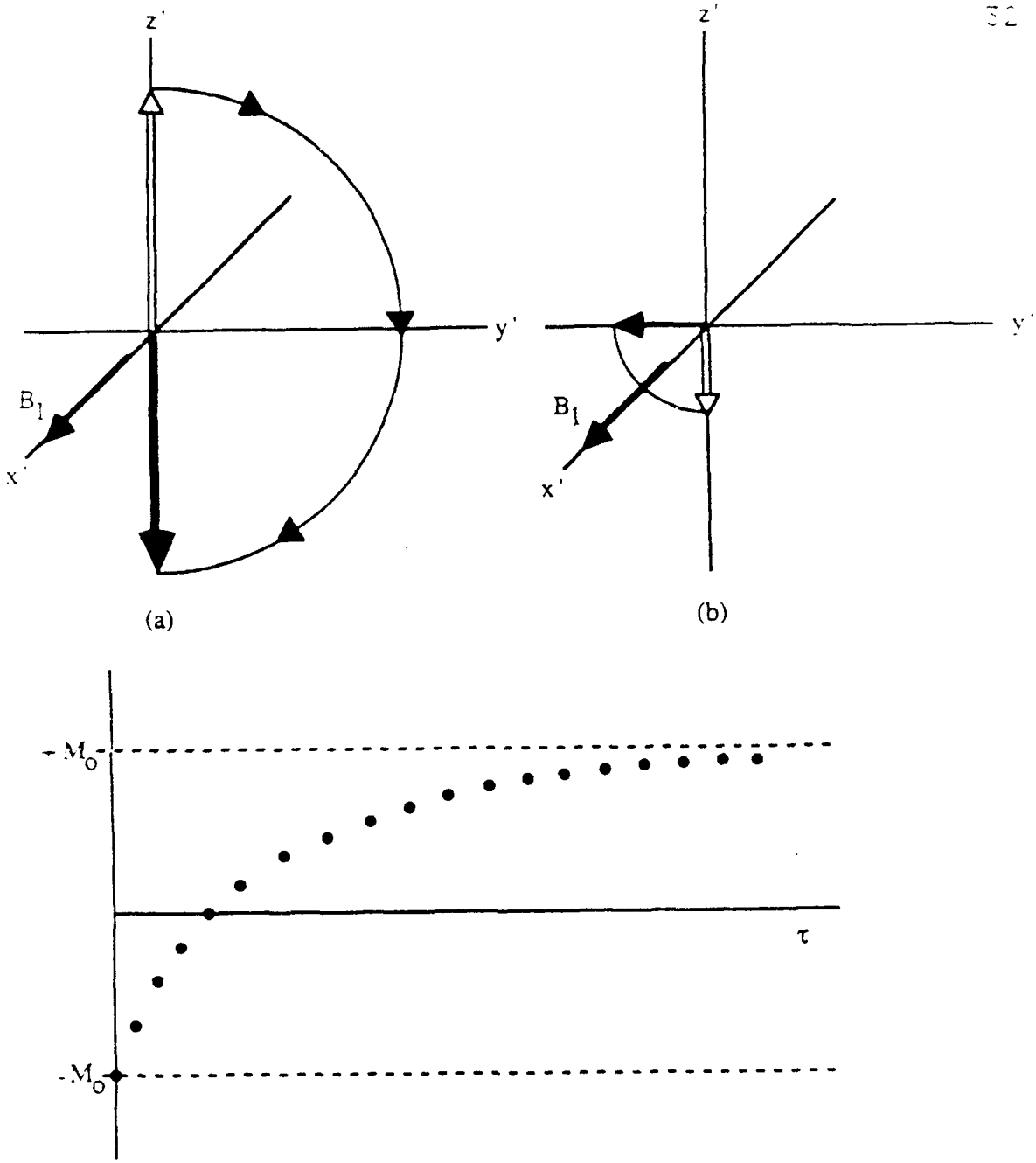

Figure 13. Determination of T_1 by 180°, τ , 90° sequence.

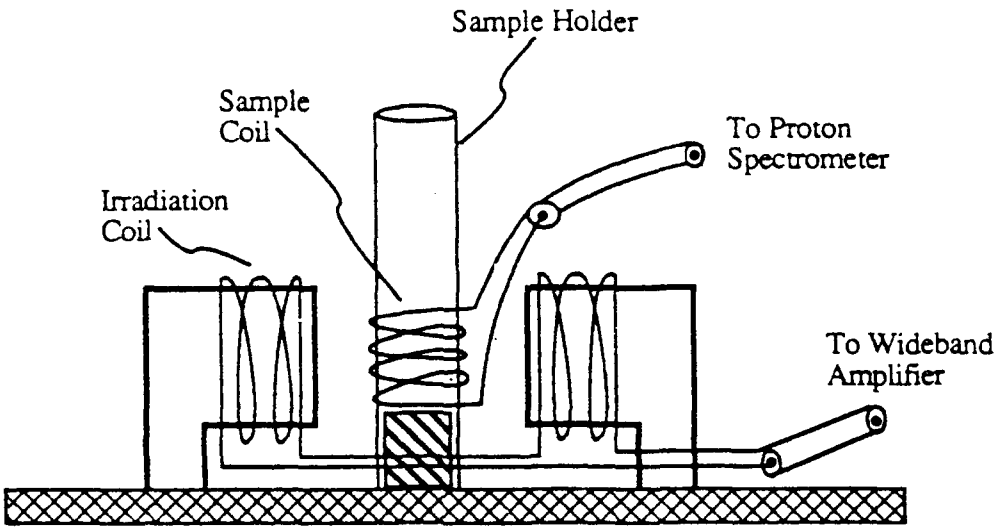

Figure 14. Detail of crossed-coil double irradiation probe.

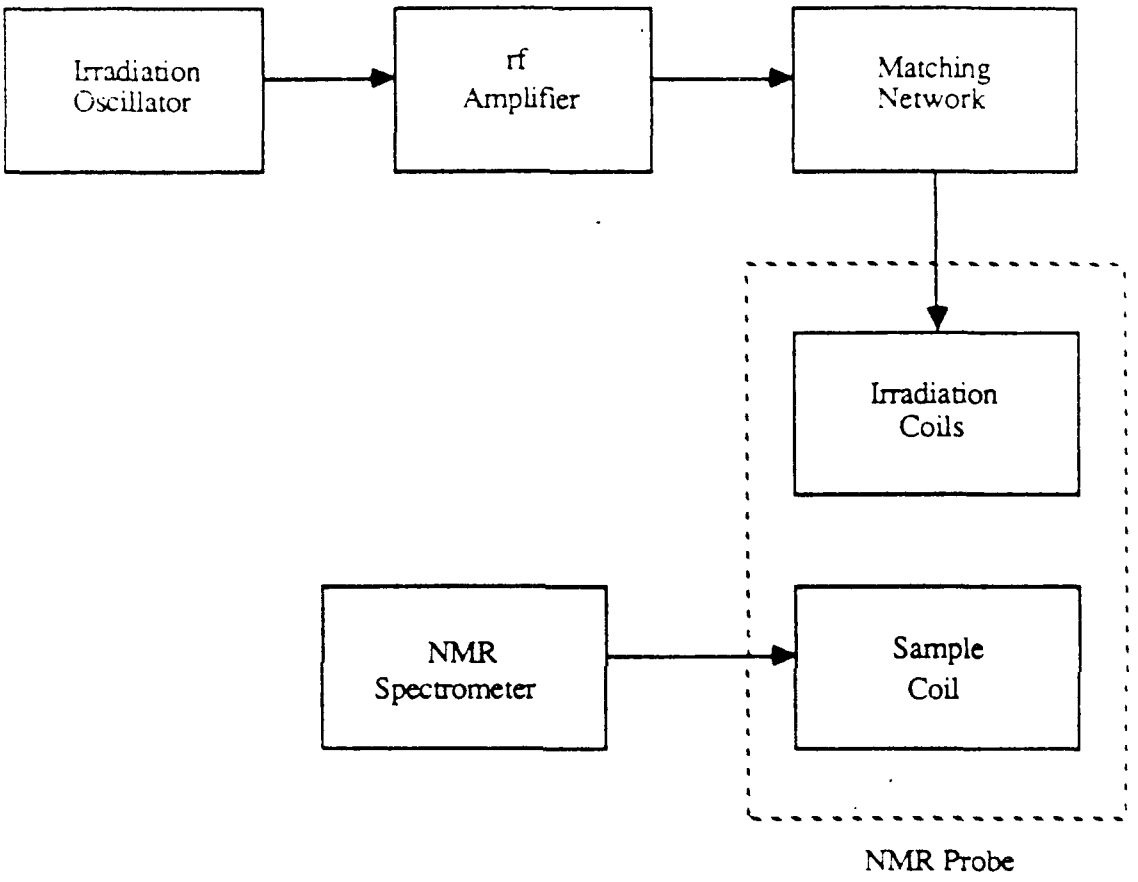

Figure 15. Block diagram of two-coil double irradiation system.

coils to a minimum, the axes of the coils were designed so that they would be at right angles.

The irradiation of the sample was accomplished by applying rf pulses from a Matec pulse amplifier. The Matec had a peak output power of one kilowatt and a duty factor of .005. The problem with this technique was that the average output power of the amplifier was five watts or less. When the amplifier delivered full power and the pulse duration (t_p) was five microseconds, the pumping power was delivered over a bandwidth of about 200 kilohertz. Although it was difficult to make precise measurements of the rf pumping effects, this procedure did indicate that the irradiation could induce the desired transitions. This in turn demonstrated that our basic approach to the problem was worth pursuing.

The pulse technique employed at this phase of the experiment is shown in the timing diagram of Figure 16. In this method a series of rf pulses of duration t_p and spacing t_s are applied during the time that the sample is returning to equilibrium. Several of these signals are then averaged to provide a comparison between FID's with irradiation and those without.

There is a potentially serious drawback to this form of irradiation. As was mentioned earlier, while the carrier frequency of the rf pulses is centered on the desired pumping frequency, the short finite pulse length produces irradiation over a band of frequencies rather than at a single frequency. Although this was not a problem in the demonstration of the feasability of the project, it made the determination of frequency effects impossible to observe. This, in turn, caused a great deal of difficulty in the interpretation of the results.

At this point, it was decided that the pulse technique would be abandoned in favor of the countinuous wave (CW) technique. The principal advantages of the CW technique

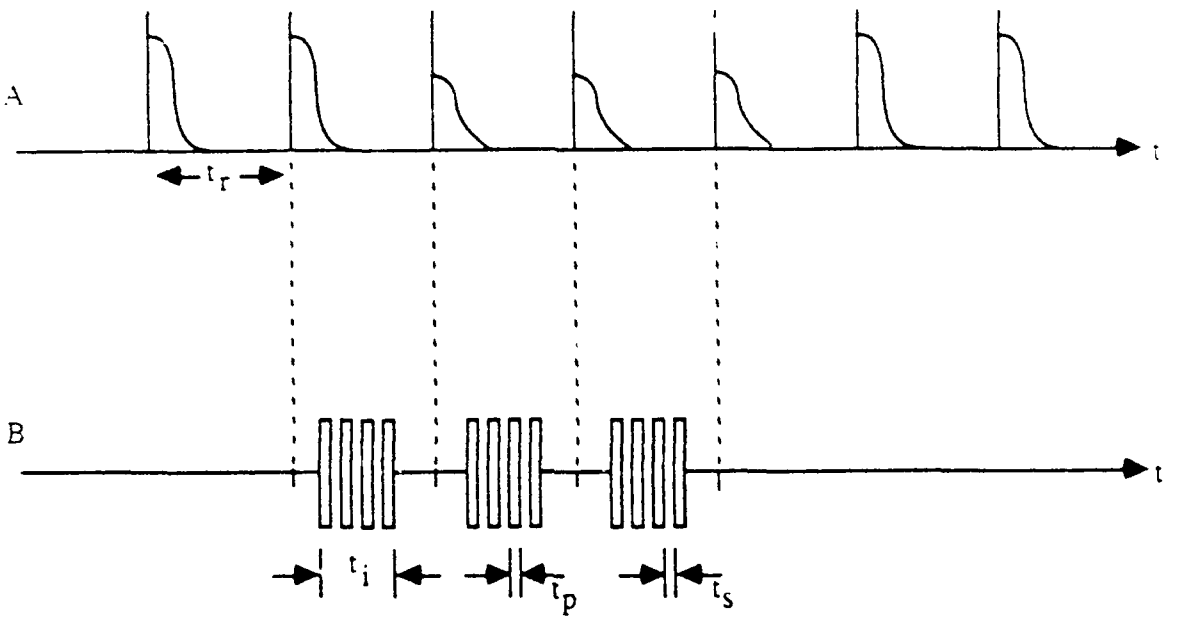

Figure 16. Timing diagram for the pulse-train experiment with pulse rf pumping. A: Proton FID; B: Off-Resonance pumping.

are that the irradiation frequency is well defined and that the peak power in the probe circuit is equal to the average power delivered. The CW technique was then used for the duration of the research.

For the initial CW studies, the crossed-coil probe was employed. However, probes other than the crossed-coil probe were subsequently investigated. Since the system remained basically unchanged (except for the probe) for the duration of the experimental work, a short description of the equipment is given below.

The pulse NMR spectrometer is a Spin-Lock Electronics Model CPS-2 operating at a Larmor frequency of 19.14 MHz. Used in conjunction with an Hitachi Model 6041 digital oscilloscope, it is essentially equivalent to the system shown in Figure 13. The irradiation electronics consists of a PTS 160 frequency synthesizer, an Amplifier Research Model 150LA rf power amplifier, and a Diawa CL-680 impedance matching circuit. A variable length of coaxial cable is used to bring the impedance of the sample circuit within the range of the coupling circuit.

The determination of the effects of off-resonance CW pumping were accomplished through two methods, single-pulse and multiple-pulse. A timing diagram for the single-pulse method is shown in Figure 17. First, the experiment is performed without pumping as shown in Figure 17a. At time zero, the spin system is prepared by using a sequence of 90° pulses (a "bash" sequence) which sets the nuclear magnetization to zero. Immediately following the bash sequence the magnetization grows, with characteristic time T_1, toward its equilibrium value M_0. After a time t_r, which should be approximately $5T_1$'s, a single 90° pulse is applied at the proton Larmor frequency and the FID is recorded. This procedure is repeated several times so that an average value can be obtained.

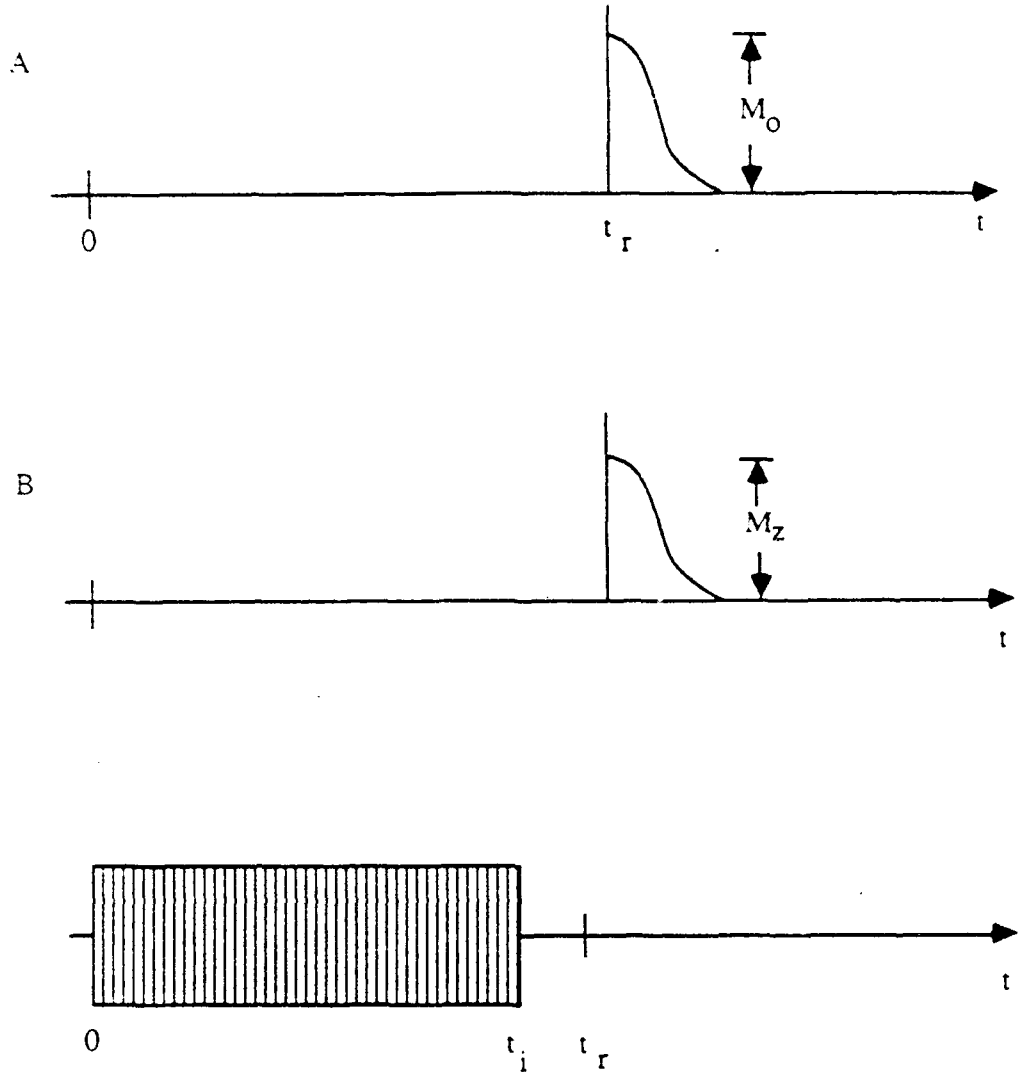

Figure 17. Timing diagram for single-pulse rf pumping experiment.
A: Measurement of equilibrium magnetization;
B: Effect of off-resonance pumping.

The experiment is then repeated with the following change. As shown in Figure 17b, rf pumping is applied to the spin system in the interval between time zero and time t_r. If the frequency of the rf pumping corresponds to one of the allowed or weakly-allowed transitions discussed in Chapter 2, and if the rf power is sufficient to stimulate a significant number of transitions at this frequency, then the populations of the proton states will be altered. Since the times required for this procedure were so long, a simpler procedure was investigated.

A timing diagram for the multiple-pulse method of determining the effects of off-resonance pumping is shown in Figure 18. In essence, this method is equivalent to the single-pulse method except it has the advantage that t_r is much shorter than $5T_1$'s.

As shown in Figure 18, a series of 90° pulses is applied to the proton spin system at the Larmor frequency. The magnitude of the FID signal after each pulse depends only upon the pulse spacing if the pulses are good 90° pulses.

In a typical measurement sequence without any irradiation, the FID signals after a set of several pulses are recorded and averaged to provide an amplitude reading. Then a bash sequence is applied so that the magnetization is set to zero. Now the sample is irradiated with the rf pumping between the 90° pulses. The FID signals are again recorded and averaged, and the amplitude reading with pumping is compared to the amplitude reading without pumping. The percentage change as a function of pumping frequency, at a constant field, provides a signature for the compound under study.

Despite considerable effort to eliminate it, dielectric heating of the sample was experienced with the crossed-coil probe which caused a detuning problem in the spectrometer circuit. This dielectric heating was serious enough to mask any effects that the irradiation might have induced. Therefore, the probe configuration was altered.

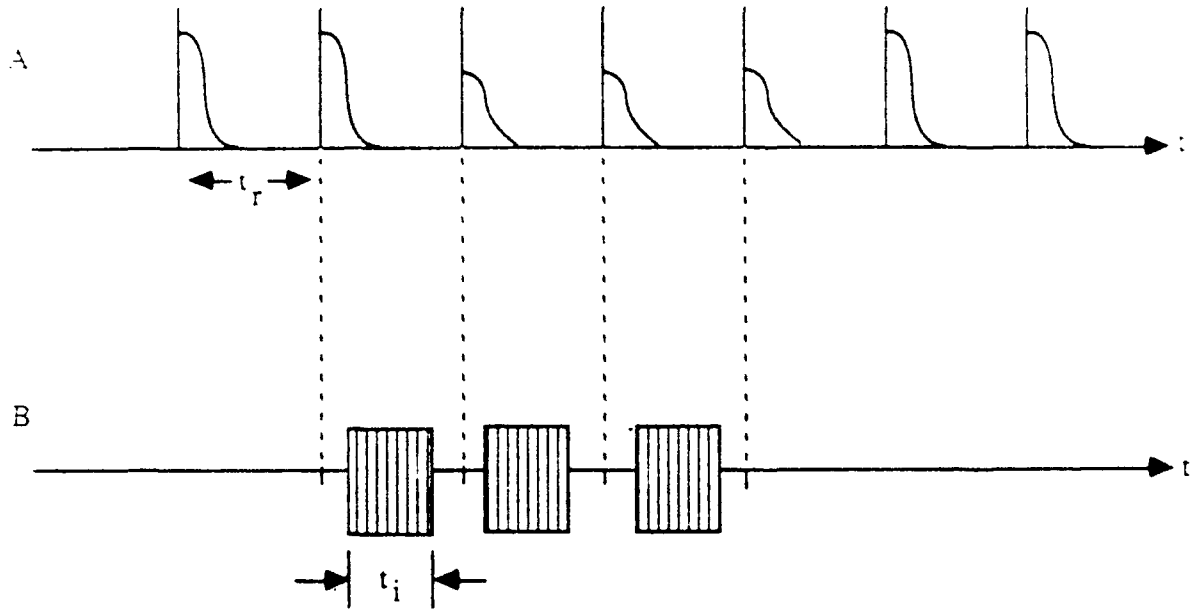

Figure 18. Timing diagram for the pulse-train experiment with cw rf pumping.
A: Proton FID; B: Off-Resonance pumping.

The first change was to a single-coil probe. The block diagram of the single-coil double-irradiation system is shown in Figure 19. In this system the series-tuned sample circuit is connected through a quarter wavelength of coaxial cable to the NMR spectrometer. A coaxial switch allows the sample circuit to be disconnected from the NMR spectrometer and connected to the pumping electronics. Matching of the sample coil to the NMR spectrometer is critical and small changes in the inductance produce large changes in both the magnitude of the received signal and the signal-to-noise ratio.

In the single-coil configuration the temperature of the sample could not be held constant. To remedy this, the sample was immersed in a Freon bath. However, this introduced additional complexities and made the probe very difficult to tune. The single-coil probe was then abandoned in favor of a sufficient two-coil solution.

At this point a probe with coaxial coils was investigated using the principles set forth by Mansfield and Chapman (21). Although this design produced the expected increase in power efficiency, the strong coupling between the coils caused serious heating of the sample, and thus detuning problems.

Due to the failures of the above mentioned probe designs, it was decided to try two parallel coils which were isolated from one another. A sketch of the final probe is shown in Figure 20. To insure that there would be no heating of the sample, high pressure air was used to carry heat away from the irradiation coil. These modifications were sufficient to solve both the heating and detuning problems.

The probe was fabricated by taking two pieces of 3/4 inch diameter brass tubing approximately 4 inches long and silver soldering them together. It is important to have the brass tubing pieces firmly connected so there will be no acoustic ringing in the NMR circuitry. Two separate but identical coils were then designed and placed in the center of the tubes.

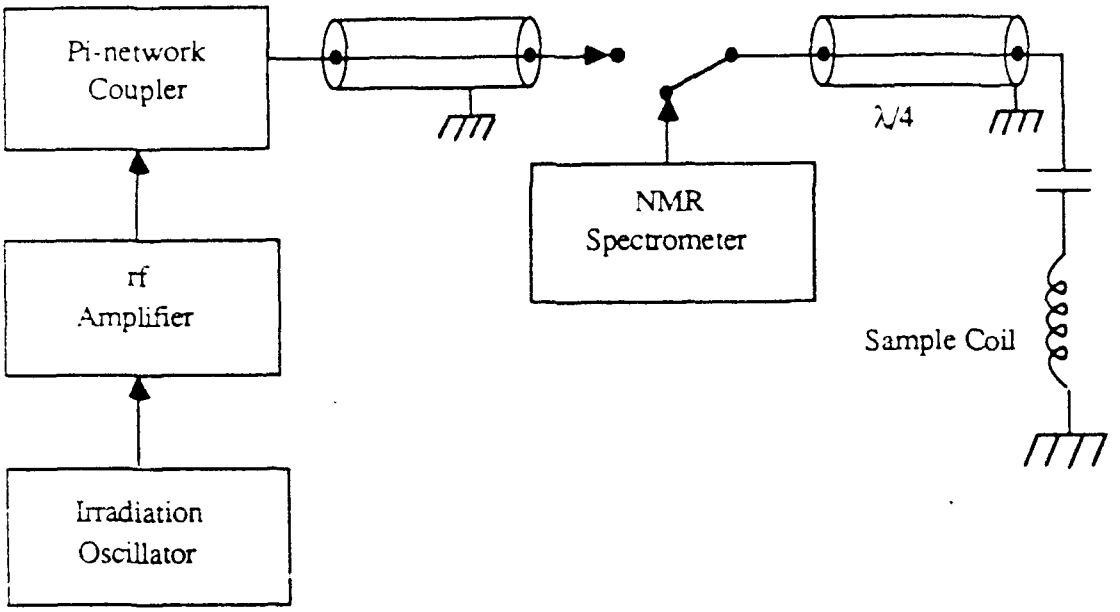

Figure 19. Block diagram of single-coil double-irradiation system.

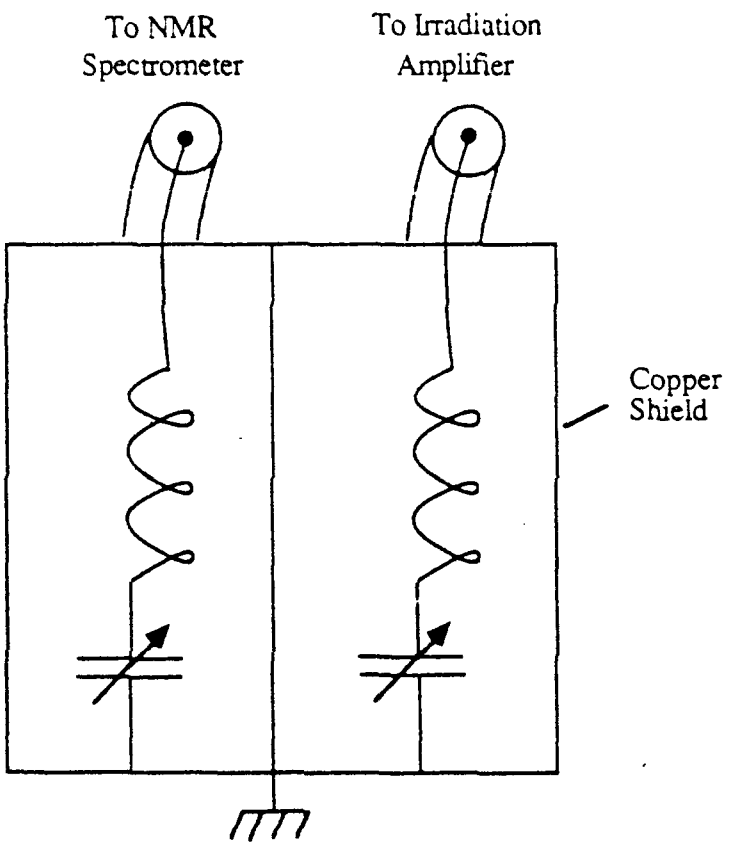

Figure 20. Detail of two-compartment double-irradiation probe.

Although this probe eliminated any detuning problems due to dielectric heating, the sample had to be physically moved from one coil to the other during the experiment. At least two sample moves per measurement sequence are required. However, since the spin-lattice relaxation times of all the compounds of interest were long, this requirement represented a minor inconvenience at worst.

Irradiation Power

Since the effects of the irradiation at different frequencies have to be compared to see the overall effect of off resonance pumping, it is important to make sure that the strength of the irradiation field remains constant.

The magnetic field produced by the pumping is time varying and is given by

$$B = B_{1b}\sin(\omega_b t).$$

From basic electromagnetism the voltage induced in a circuit is given by

$$V_I \propto \frac{d\Phi}{dt} = A\frac{dB}{dt} = AB_{1b}\omega_b\cos(\omega_b t)$$

where A = constant, ω_b is the irradiation frequency, and B_{1b} is the field that is to be held constant. Therefore,

$$B_{1b} \propto \frac{V_I}{\omega_b}.$$

Throughout the experiment the induced voltage (V_I), as measured by a small four-turn pickup coil six millimeters in diameter, was chosen to be 60 Volts at a frequency of 24 MHz.

CHAPTER IV

RESULTS

Introduction

In this chapter the details of the experiments, along with the results obtained, are discussed. As indicated in the last section, not all of the probes that were designed and constructed worked satisfactorily. Therefore, when the term "probe" is used in this chapter it is assumed that it is referring to the double irradiation probe that is shown in Figure 20.

The multiple pulse method of data acquisition was used in conjunction with continuous wave irradiation to map out the effects of off-resonance pumping as a function of frequency. The exact method varied slightly for each compound due to the different T_1's, but the specifics will be discussed later.

The Compounds

The molecular structure of hexemethylenetetramine (HMT) is shown in Figure 21. It consists of four nitrogen atoms, six carbon atoms, and twelve hydrogen atoms per molecule. Therefore, HMT contains a substantial fraction of nitrogen nuclei which are closely coupled to the protons. The bonding angles and distances are well known and given in many references (22).

At a proton Larmor frequency of 19.14 MHz (1.38 MHz for nitrogen), HMT has a T_1 (spin-lattice relaxation time) of 58 seconds, and a T_2 (spin-spin relaxation time) of approximately two microseconds, as measured in our laboratory. If the sample is at room temperature, the NQR frequency is found to be 3.308 MHz (23). The nitrogen

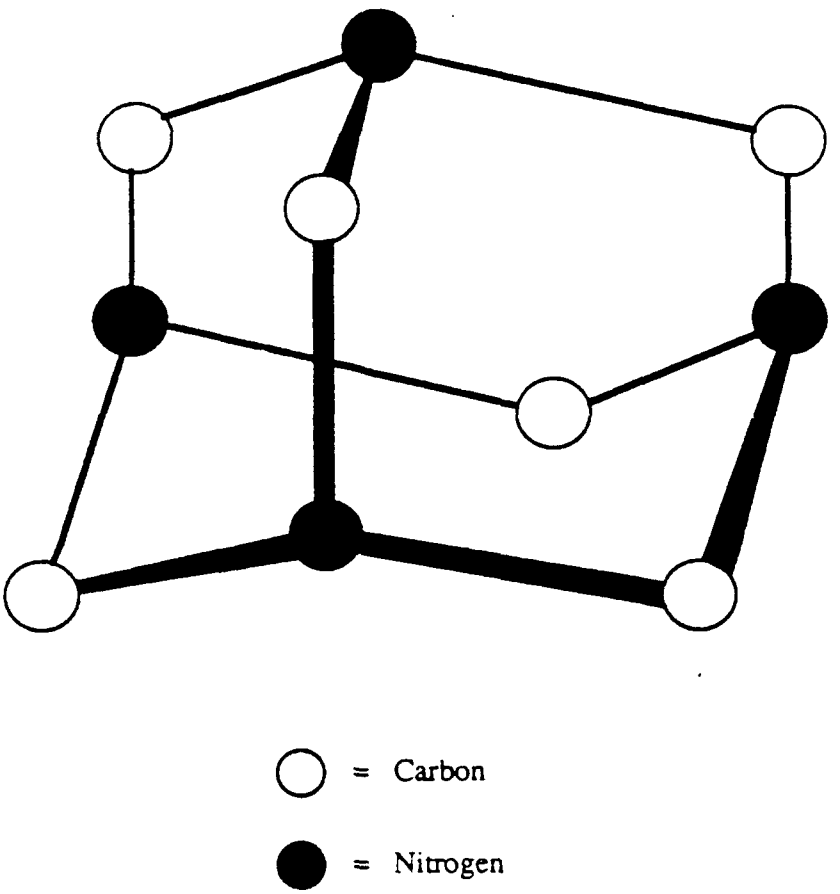

Each carbon atom is bonded to two hydrogen.

Figure 21. Molecular structure of hexamethylenetetramine.

T_1 in zero field is about 10 milliseconds (24), and the nitrogen T_2 is about 500 microseconds (25). These short relaxation times indicate that the populations of the nitrogen energy levels return to equilibrium much faster than the populations of the proton energy levels.

There are many compounds that do not contain substantial amounts of nitrogen. Therefore, the spin coupling effects characteristic of nitrogen-containing compounds, which is what is under study in this project, are absent. Therefore, it should be quite easy to find a suitable compound to compare to the HMT.

For comparison of the results from HMT, a compound had to be chosen that had a T_1 comparable to, or longer than, HMT. The compound that was finally chosen was mannitol, a complex sugar. The chemical structure of mannitol is depicted in Figure 22.

Mannitol consists of a six-carbon linear chain, with one hydroxol group on each carbon. At a Larmor frequency of 19.14 MHz, the T_1 of mannitol is approximately 280 seconds while the T_2 is approximately 4.5 microseconds (26).

HMT Results

As was stated earlier, there were many techniques employed to attempt and map the effects of off-resonance pumping as a function of frequency. Most of these techniques had serious drawbacks and have already been discussed. However, reliable data was finally obtained in the following manner.

First, a series of closely-spaced 90° pulses was applied to set the proton magnetization to zero. Then, the sample was allowed 30 seconds to recover toward its equilibrium value. Then a series of four 90° pulses was applied to the sample with a spacing of 30 seconds. This sequence of events is depicted in Figure 23a.

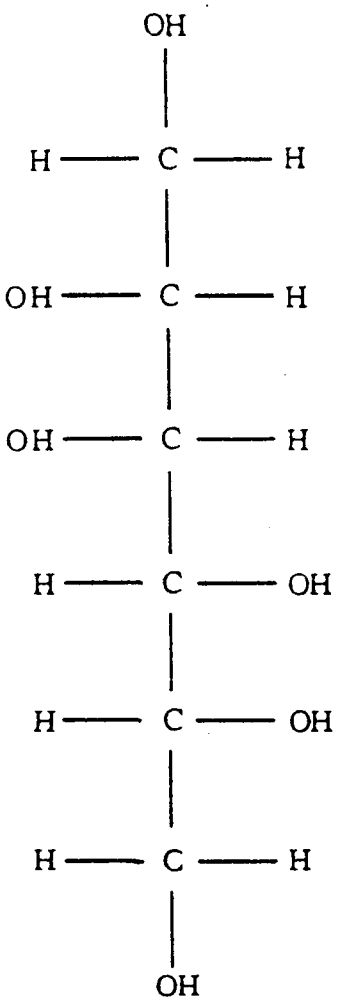

Figure 22. Molecular structure of mannitol.

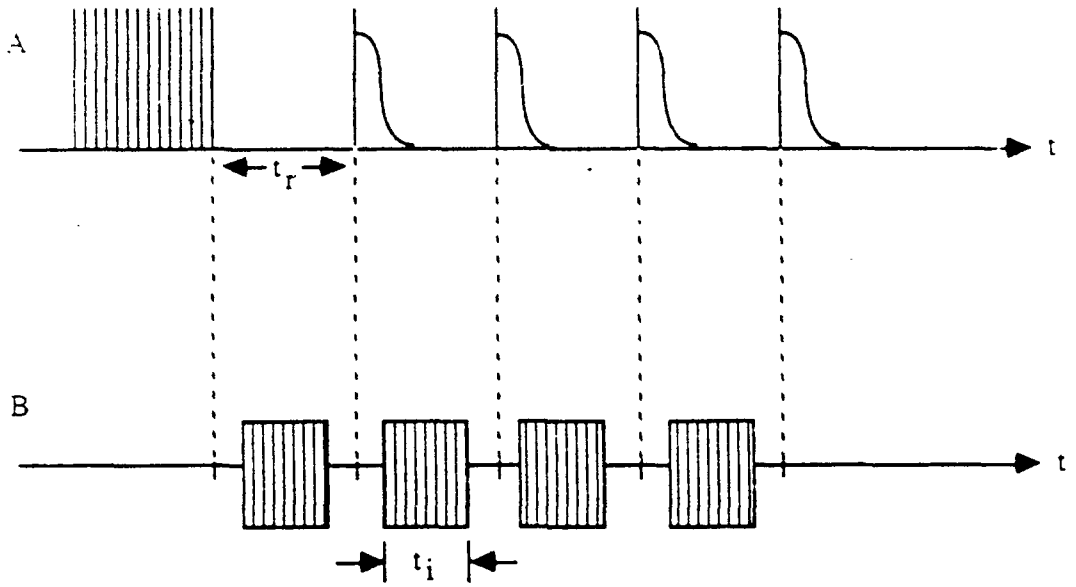

Figure 23. Timing diagram for multiple-pulse rf pumping experiment.
A: Proton FID; B: Off-Resonance pumping.

The free induction decays (FID's) following each of the four pulses were stored and averaged, and the magnitude of the average FID at a specific time delay from the start of the pulse was recorded.

The same sequence was then repeated with rf irradiation applied at a particular frequency between the 90° pulses. This is shown in Figure 23b. The rf pumping power was applied for a time of 20 seconds during the 30-second interval between the pulses. The magnitude of the averaged FID with irradiation, at the same time delay, was recorded.

The above sequence, without pumping and then with pumping, was repeated four times and averaged by hand. Then the results obtained with and without pumping were compared and the percentage decrease due to pumping was calculated. The experiment was then repeated for other pumping frequencies and the results mapped out as a function of frequency.

The final results of this procedure for HMT are given in Table 2. It must be noted that the percent decreases given in the table are averages of many data values. Not only were the four FID's averaged after the 90° pulses by the oscilloscope, but the four runs were averaged to give the number presented in the percent decrease column.

The results of the data given in Table 2 are shown in Figure 24. This is a plot of the percentage decrease in proton signal amplitude due to off-resonance pumping versus the rf pumping frequency. As seen from this figure, the frequency range investigated is about 10 MHz.

As expected, the effects of pumping are greatest near the proton Larmor frequency of 19.14 MHz. The observed pumping effects near the proton Larmor frequency were attributed to the breadth of the HMT resonance line. However, significant pumping effects are observable at frequencies more than 4.5 MHz away from the proton

Table 2. Percent decrease versus pumping frequency for hexemethylenetetramine.

Pumping Frequency (MHz)	Perecent Decrease	Standard Deviation
16.4	4.6	2.4
16.5	7.7	2.7
16.6	8.9	3.4
16.8	10.8	1.7
17.0	6.1	5.8
17.1	5.8	4.4
17.2	8.6	2.1
17.4	16.2	2.8
17.6	6.0	6.9
17.7	5.9	3.6
17.8	0.0	4.1
18.0	10.1	3.6
18.4	19.9	7.0
18.8	36.7	1.0
19.0	72.9	0.2
19.2	81.1	0.7
19.4	57.9	3.0
19.6	26.2	2.6
19.8	15.2	3.4
20.0	12.1	3.3
20.2	10.0	3.0
20.4	2.1	4.2
20.6	-0.2	8.2
20.8	6.4	2.7
21.0	1.6	2.8
21.2	6.8	2.9
21.4	5.7	5.7
21.6	1.1	1.9
21.7	0.0	0.0
21.8	4.9	4.3
22.0	4.7	5.7
22.2	8.5	4.5
22.4	5.2	1.4
22.6	3.9	4.9
22.8	7.4	3.2
23.0	-3.0	6.5
23.1	0.0	0.0
23.2	-2.0	2.2
23.4	-1.5	3.9
23.6	5.8	2.6
23.8	12.2	3.7
24.0	1.2	1.2
24.5	0.6	3.9
25.0	0.0	1.2
25.5	0.0	2.2

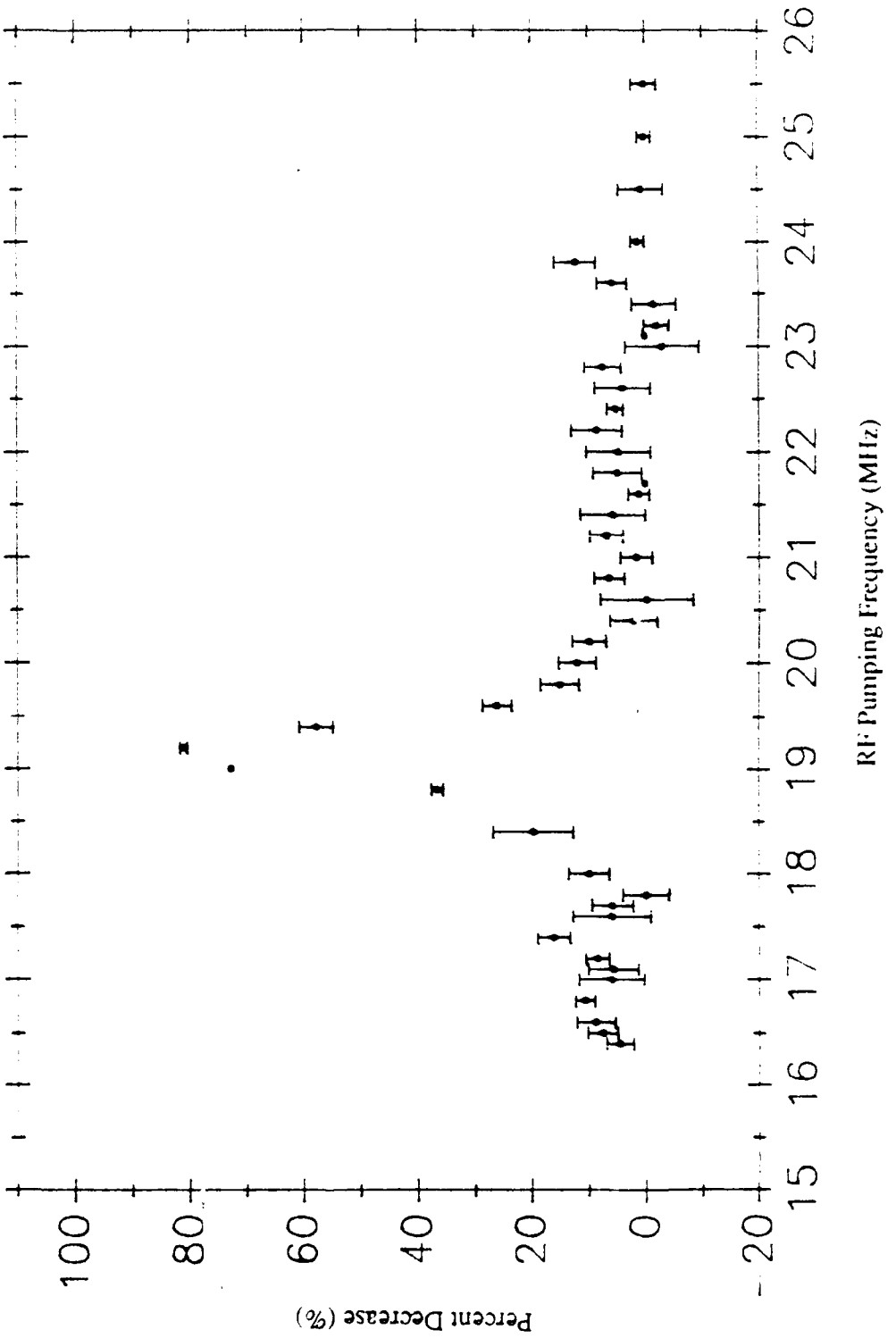

Figure 24. Percent decrease versus rf pumping frequency in hexamethylenetetramine.

resonance. In fact, a peak in the observed response appears to occur at about 23.8 MHz, just before the response drops to zero at 24.0 MHz.

If numerical values are assigned to the energy levels of Figure 10 for the low field approximation, a prediction of zero response to rf pumping above 23.74 MHz is obtained. This is the same value that can be derived from the high field approximation as shown in Figure 12. Therefore, there is qualitative agreement between the experimental results and the theoretical framework.

As was mentioned several times, the data in Figure 24 represents the results of many trials. However, the error bars do not have the usual meaning. This is due to the fact that the oscilloscope did not allow the inspection of each of the four FID's that were averaged. Therefore, the uncertainty in the individual FID measurements is not known. What the error bars in Figure 24 represent are the standard deviations in the trials that consisted of the four FID's averaged by the oscilloscope.

Careful inspection of Figure 24 reveals that the effect is not a simple function of frequency. There appear to be both minima and maxima located throughout the frequency range. As seen from the data in Table 2, there are definite regions of zero response near 21.7 MHz and 23.1MHz. There was much time spent in the acquisition of data in these two regions. Instead of the normal four data runs, there were 12 runs for each point. Although much effort was spent in trying to explain this complex behavior, no satisfactory theory was derived.

Examining the data in Table 2, the change in the apparent T_1 can be investigated. That is, a 12% decrease (observed at 23.8 MHz) corresponds to a change in T_1 from 60 seconds (no rf pumping), to approximately 71 seconds when the sample is irradiated.

Mannitol Results

The procedure for obtaining the mannitol data is identical to that for obtaining the HMT data, except that the time between pulses was extended to 60 seconds. This change was made because the T_1 for mannitol is approximately five times longer than the T_1 for HMT. This resulted in a signal that was too small to read accurately when only a 30- second delay was used.

The data for the mannitol sample are shown in Table 3, and these data are plotted in Figure 25. Again, this is a plot of the percentage decrease in proton signal amplitude versus rf pumping frequency over a frequency range of seven megahertz.

As in the HMT, the effect is largest near the proton Larmor frequency of 19.14 MHz. However, unlike the HMT, there are no noticeable effects due to rf pumping more than a megahertz away from the proton Larmor frequency.

The lack of effects in the mannitol is attributed to the fact that there are no nitrogen nuclei in the sample and, hence, no hydrogen-nitrogen couplings. The energy level diagram needed to explain the data is that of a simple two-level system and there are no weakly-allowed transitions to stimulate off-resonance pumping.

Conclusion

This research demonstrated that it was possible to induce weakly-allowed transitions through off-resonance rf pumping. By analyzing the data it was found that, on the average, a 10% decrease in the proton FID amplitude was obtainable in HMT more than four megahertz from the proton Larmor frequency. Though this data was not simple to interpret, it was in qualitative agreement with the theory.

If these same effects had been observed in mannitol, the experiments would have demonstrated nothing. However, this was not the case. After only one megahertz, there was no change in the proton FID due to rf pumping.

Table 3. Percent decrease versus pumping frequency for mannitol.

Pumping Frequency (MHz)	Perecent Decrease	Standard Deviation
16.0	0.6	1.3
16.5	-0.1	1.9
16.8	1.4	2.0
17.5	0.9	1.4
17.6	-0.1	3.2
17.9	-0.6	4.1
18.5	8.0	8.5
18.8	16.4	1.6
19.1	99.2	1.4
19.4	41.6	6.2
19.7	17.6	4.5
20.0	4.4	11.6
20.3	-0.2	3.4
20.6	-0.6	3.0
20.9	-2.2	5.7
21.2	0.6	2.2
21.5	1.1	2.9
22.0	1.6	2.6
22.2	0.1	1.6
22.5	0.7	2.3
23.0	-0.4	1.8

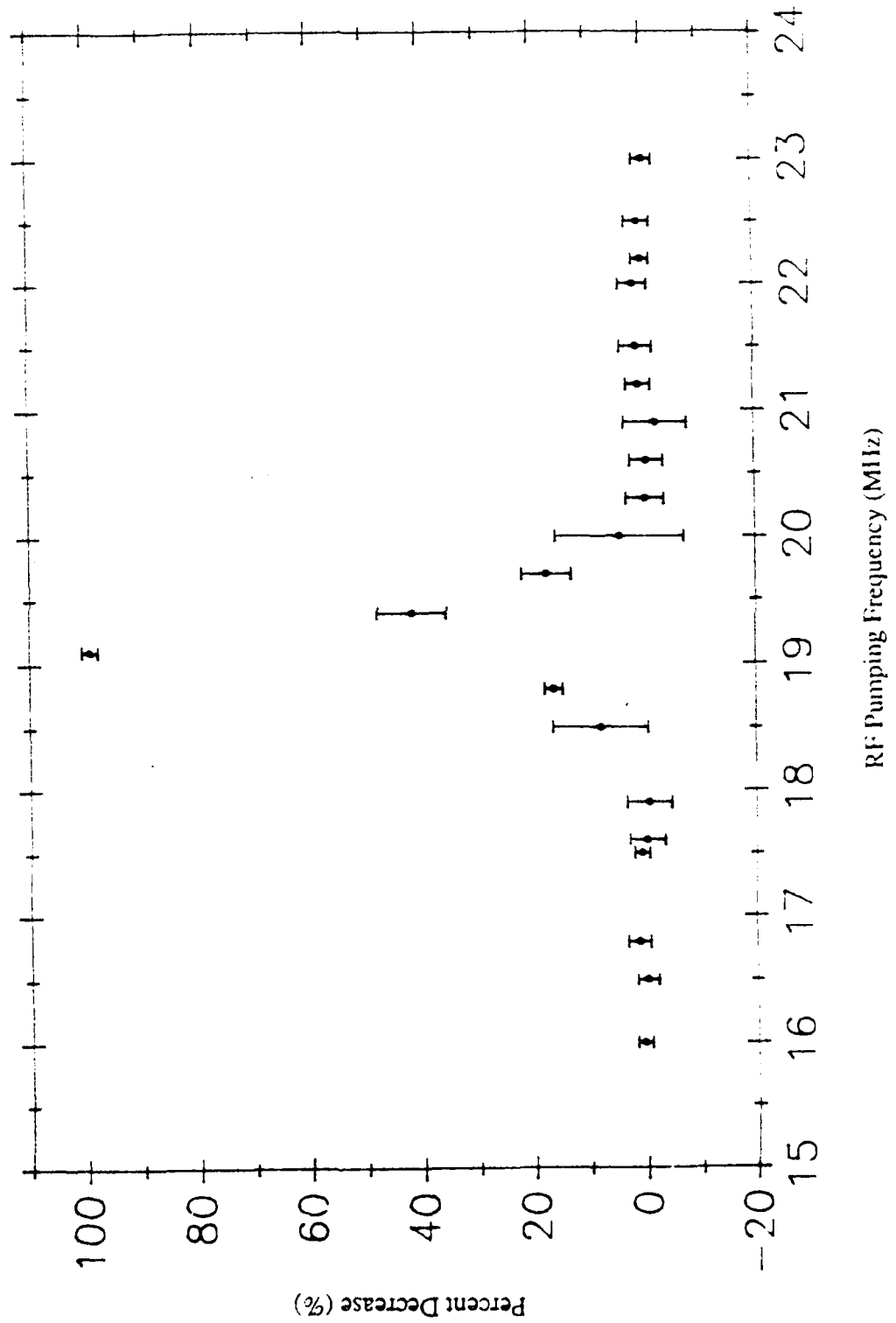

Figure 25. Percent decrease versus rf pumping frequency in mannitol.

This technique could open up new means for identifying classes of compounds by NMR. There is also the possibilty of identifying the compound itself if unique signatures are observed within the classes. This in itself should be a major reason for trying to understand the frequency effects that were observed in the HMT.

REFERENCES

REFERENCES

(1) A. Abragam, The Principles of Nuclear Magnetism, (Oxford University Press, Amen House, London, 1961)

(2) C. P. Slichter, Principles of Magnetic Resonance, (Springer-Verlag, Berlin, 1978)

(3) T. C. Farrar and E. D. Becker, Pulse and Fourier Transform NMR (Introduction to Theory and Methods), (Academic Press, New York, 1971)

(4) E. Fukashima and S. B. W. Roeder, Experimental Pulse NMR, A Nuts and Bolts Approach, (Addison-Wesley, Reading, MA, 1981)

(5) Reference (2), Chapter 1, p. 2

(6) Ibid

(7) E. R. Andrew, Nuclear Magnetic Resonance, (Cambridge University Press, London, 1958), Chapter 2, p. 8

(8) Reference (2), Chapter 1, pp. 4-10

(9) L. Burnett, J. Sanders, and M. Fineman, "Nuclear Magnetic Resonance for Remote Detection Applications", EG&G Incorporated, Final Report on Contract Number J6121, September 1987

(10) Reference (3), Chapter 4, p.

(11) Reference (1), Chapter 7, pp. 232-261

(12) Reference (2), Chapter 9, pp. 288-291

(13) E. A. C. Lucken, Nuclear Quadrupole Coupling Constants, (Academic Press, New York, 1969)

(14) H. G. Dehmelt, Journal of American Physics, 22 (3), 110 (1954)

(15) R. Tycko and S. J. Opella, Journal of American Chemical Society, 108, 3531 (1986)

(16) P. A. Fedders and P. C. Sayers, Physical Review B, 35 (7), 3088 (1987)

(17) Reference (1), Chapter 9, p. 395

(18) R. A. Wind and C. S. Yannoni, Journal of Magnetic Resonance, 72, 108 (1987)

(19) Reference (1), Chapter 7, p. 232

(20) Reference (3), Chapter 2, p. 21

(21) P. Mansfield and B. Chapman, Journal of Magnetic Resonance, 72, 211 (1987)

(22) G. W. Smith, Journal of Chemical Physics, 36 (11), 3081 (1962)

(23) W. C. Rollwitz, private communication

(24) S. Alexander and A. Tzalmona, Physical Review, 138, 4845 (1965)

(25) R. J. Trepanier and M. A. Whitehead, Journal of the Chemical Society, Faraday Transactions 2, 82, 115 (1986)

(26) L. J. Burnett, "A Study to Evaluate Nuclear Magnetic Resonance for Narcotics Detection", U. S. Customs, Final Report on Contract Number CS-085-2075-1, April 1986

ABSTRACT

ABSTRACT

The effects of off-resonance irradiation in the NMR of solids was investigated using two classes of compounds. The first class consisted of those compounds that contained nitrogen (that is, nitrogen-14), while the second class consisted of those compounds without nitrogen.

The two compounds investigated, representing members of each class mentioned above, were hexemethylenetetramine (HMT) and mannitol. The first, HMT, contains nitrogen, while the second, the sugar mannitol, contains no nitrogen.

The stimulation of the weakly-allowed transitions were investigated by comparing the proton FID amplitudes at a particular time delay. This was accomplished through the comparison of an FID that was taken after the sample had been irradiated, to an FID that was taken from a sample that was not irradiated. Using this technique it was possible to map out the percent change in the proton FID amplitude as a function of the rf pumping frequency.

By analyzing the data it was found that, on the average, a 10% decrease in the proton FID amplitude was observable in HMT more than four megahertz from the proton Larmor frequency. However, this was not the case for the mannitol. In the mannitol data, there was no change in the proton FID amplitude more than one megahertz from the proton Larmor frequency.

The views and conclusions contained in this report are those of the cor :ractors and should not be interpreted as representing the official policies, either expressed or implied, of the Naval Ocean Systems Center or the U.S. Government.

Approved for public release; distribution is unlimited.